Molecular Cell

Article

The essential co-chaperone Sgt1 regulates client dwell time in the Hsp90 chaperone cycle

Graphical abstract

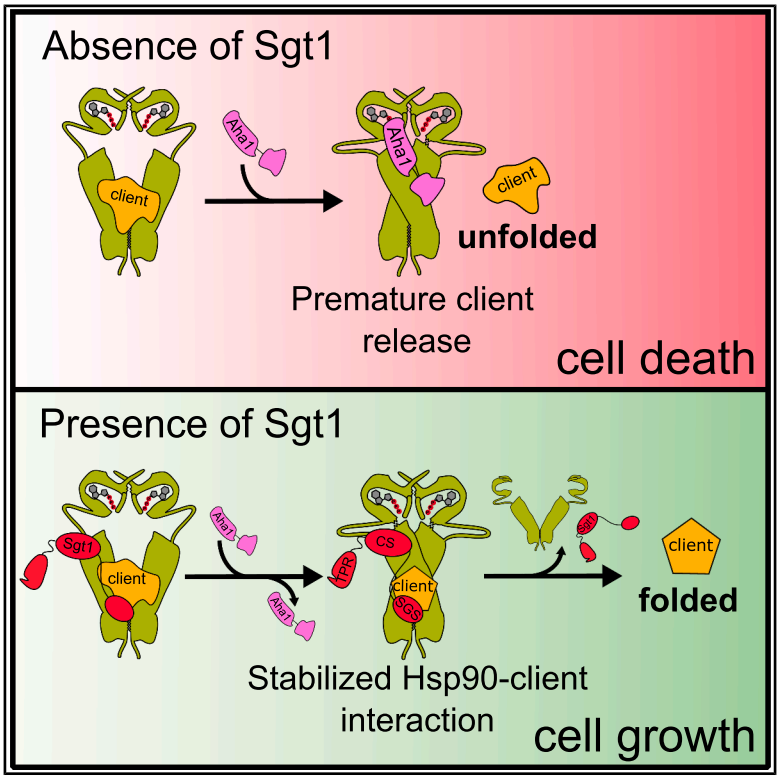

Highlights

- Sgt1 has a general function in the Hsp90 cycle
- The Sgt1-specific SGS domain is essential and required for Sgt1's chaperone function
- The CS domain of Sgt1 binds to the middle domain of Hsp90, and the SGS binds to clients
- Sgt1 stabilizes Hsp90-client complexes and prevents their dissociation mediated by Aha1

Authors

Sonja Engler, Florent Delhommel, Christopher Dodt, ..., Rina Rosenzweig, Michael Sattler, Johannes Buchner

Correspondence

michael.sattler@tum.de (M.S.), johannes.buchner@tum.de (J.B.)

In brief

Engler et al. define the Sgt1-specific domain as essential for the Sgt1 chaperone function in yeast. Through structural and biochemical analyses, they uncover unique interactions of Sgt1 with Hsp90 and client proteins that enhance client maturation efficiency. Sgt1 stabilizes Hsp90-client complexes by preventing their dissociation mediated by the co-chaperone Aha1.

Engler et al., 2026, Molecular Cell *86*, 166–179
January 8, 2026
https://doi.org/10.1016/j.molcel.2025.12.002

CellPress

CellPress
OPEN ACCESS

Molecular Cell

Article

The essential co-chaperone Sgt1 regulates client dwell time in the Hsp90 chaperone cycle

Sonja Engler,[1,5] Florent Delhommel,[2,3,5] Christopher Dodt,[1] Abraham Lopez,[2,3] Ofrah Faust,[4] Annika Elimelech,[2,3] Valeria Napolitano,[2,3] Grzegorz M. Popowicz,[2,3] Rina Rosenzweig,[4] Michael Sattler,[2,3,*] and Johannes Buchner[1,6,*]

[1]Center for Functional Protein Assemblies (CPA), Department Bioscience, TUM School of Natural Science, Technical University of Munich, Ernst-Otto-Fischer-Strasse 8, Garching, Germany

[2]Bavarian NMR Center, Department Bioscience, TUM School of Natural Science, Technical University of Munich, Ernst-Otto-Fischer-Str. 2, Garching, Germany

[3]Helmholtz Munich, Molecular Targets and Therapeutics Center, Institute of Structural Biology, Ingolstädter Landstr. 1, 85764 Neuherberg, Germany

[4]Department of Chemical and Structural Biology, Weizmann Institute of Science, Rehovot, Israel

[5]These authors contributed equally

[6]Lead contact

*Correspondence: michael.sattler@tum.de (M.S.), johannes.buchner@tum.de (J.B.)

https://doi.org/10.1016/j.molcel.2025.12.002

SUMMARY

The Hsp90 molecular chaperone system is regulated by numerous co-chaperones that modulate its function. In *Saccharomyces cerevisiae*, most of these cofactors can be deleted without affecting viability. Of the three essential ones, only the function of Sgt1 has remained enigmatic. Our *in vivo* and *in vitro* experiments define key structural elements and determine the essential function of Sgt1 in the chaperoning of client proteins. We demonstrate that yeast Sgt1 adopts a unique binding mode, engaging primarily with the middle domain of Hsp90. Through simultaneous interaction with both Hsp90 and client proteins, Sgt1 enhances client maturation efficiency. Specifically, Sgt1 stabilizes Hsp90-client complexes and prevents their dissociation by the co-chaperone Aha1. Our findings reveal a previously unrecognized layer of Hsp90 regulation, highlighting Sgt1 as a critical modulator of chaperone cycle progression.

INTRODUCTION

Cells rely on sophisticated folding machinery to deal with the constant risk of protein misfolding and aggregation.[1] A key player in this machinery is the heat shock protein 90 (Hsp90), one of the most abundant molecular chaperones in the cytosol of eukaryotic cells. It facilitates the proper folding and maturation of numerous "client" proteins, including kinases, transcription factors, signaling proteins, and cell cycle regulators.[2,3] By stabilizing these diverse clients, Hsp90 is crucial in supporting cellular signaling, growth, and stress responses.[4,5] Hsp90 consists of three domains: an N-terminal domain (NTD) linked to a middle domain (MD) via a long linker and followed by a C-terminal domain (CTD). Dimerization via the CTD results in an open, V-shaped dimer.[6,7] Driven by ATP-binding, Hsp90 undergoes large conformational changes from the open to closed states, including the dimerization of the two NTDs (closed I state), followed by the association of the NTDs with the MDs (closed II state).[7–9] These transitions are essential for Hsp90's function and are the rate-limiting step for ATP hydrolysis.

The Hsp90 homolog of *S. cerevisiae* (Hsp82, referred to as Hsp90 for simplicity's sake) works together with more than ten cofactors (also known as co-chaperones), which assist its function by diverse mechanisms.[10,11] With the exception of Hch1, all co-chaperones are conserved from yeast to humans.[12] They can interact with all three domains of Hsp90, sometimes binding simultaneously, sometimes competing with one another.[11] Although the overall interplay of co-chaperones in orchestrating the maturation of a wide range of clients is still not fully understood, decades of research have revealed how many of them modulate the Hsp90 chaperone cycle at the mechanistic level. A prominent example is Hop (Sti1 in yeast), which acts as a transfer factor, handing over clients from Hsp70 to Hsp90.[13–15] Once clients are loaded, Hop is displaced by p23 (Sba1 in yeast), which preferentially interacts with the ATP-bound state of Hsp90 and stabilizes the client-Hsp90 complex.[16–20] Both Hop and p23 slow down the ATPase cycle of Hsp90 to promote client folding.[21,22] By contrast, the co-chaperone ATPase homolog 1 (Aha1) accelerates the ATP hydrolysis of Hsp90 more than 10-fold.[23–27] While early studies reported less activation of the client protein v-Src upon Aha1 deletion in yeast,[25,28] more recent reports consistently show increased activity and stability of diverse Hsp90 clients.[26,29–32] Due to overlapping binding surfaces at the Hsp90-MD, Aha1 and some client proteins seem to compete for binding to Hsp90.[23,33,34] These findings suggest that Aha1

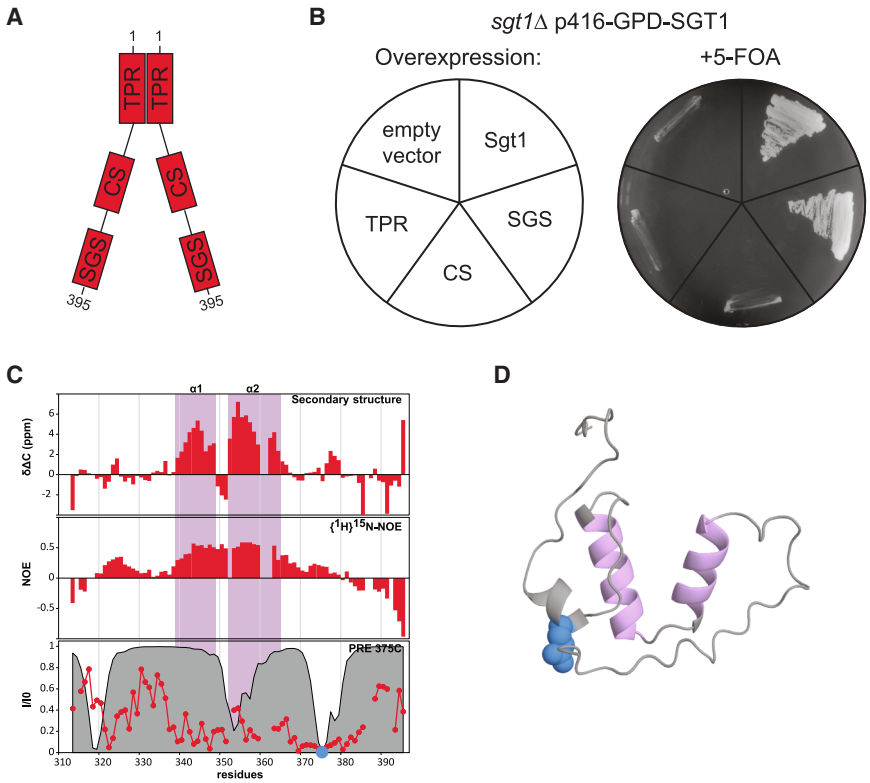

Figure 1. The SGS domain of Sgt1 performs the essential function

(A) Schematic domain architecture of Sgt1.

(B) Determination of the essential domain of Sgt1. Plasmid shuffling (right) of the *sgt1Δ* p416-GPD-SGT1 strain transformed with the empty vector (p415-GPD) or plasmids overexpressing full-length Sgt1 or Sgt1 domains as indicated (left). Transformants were streaked on 5-Fluoroorotic acid (5-FOA) plates and grown for 3 days at 30°C.

(C) The SGS domain of Sgt1 contains two stable helices, but without clear structures. Diagrams showing helical propensity (top), {1H}-15N NOE (middle), and PRE (bottom) measured with a probe introduced at position 375 (red line) compared with the predicted PRE, based on the AF2 model (gray volume).

(D) The AF2 model does not represent well the SGS structure. The AF2 model shows in pink the regions of high helical propensity determined by NMR and the position of the PRE probe in blue.

may promote client release from Hsp90, effectively "clearing" the chaperone for subsequent cycles.[35]

In yeast, only three co-chaperones are essential, one of which is the "suppressor of G2 allele of Skp1" (Sgt1). Sgt1 is conserved across all eukaryotes, with higher eukaryotes possessing two isoforms.[36–39] Structurally, Sgt1 comprises an N-terminal TPR (tetratricopeptide repeat) domain, a CS (chord-containing proteins and Sgt1) domain, and a C-terminal SGS (Sgt1-specific) domain. In yeast, Sgt1 forms dimers through the interaction of the TPR domain (Figure 1A).[40,41] With the TPR and CS domains, Sgt1 harbors two domains that are frequently used by co-chaperones to interact with Hsp90. The TPR domain, present in co-chaperones like Hop/Sti1, Cns1, and the group of large PPIases, typically recognizes the MEEVD motif at the CTD of Hsp90. Of note, a TPR domain of Sti1/Hop also interacts with the MD of Hsp90 to inhibit its ATPase activity.[42] By contrast, the CS domain, found in co-chaperones like p23/Sba1 and the human co-chaperone NudC, forms contacts with the NTD or MD of Hsp90. Unlike other Hsp90 co-chaperones, the TPR domain of Sgt1 does not seem to mediate the interaction with the C-terminal tail of Hsp90.[43,44] Instead, the CS domains of yeast,[43] plant,[45] and human[44] Sgt1 were reported to interact with Hsp90. Notably, the binding interface has only been defined for plant Sgt1 on the NTD of Hsp90, whereas it remains unresolved for yeast and human Sgt1.[45] While the TPR and CS domains are widespread, the SGS domain is nearly unique to Sgt1 and otherwise only found in the calcyclin-binding protein CacyBP.[46] Although the other Sgt1 domains are structurally resolved, the SGS domain lacks a defined structure and appears largely unstructured with small regions of helical propensity.[44] Notably, the human and plant SGS domain was reported to bind to the molecular chaperone Hsp70 rather than Hsp90, potentially linking the two chaperone systems.[47,48]

A well-studied client of Sgt1 is Skp1. Through TPR-mediated binding, Sgt1 contributes to kinetochore assembly and the Skp1/Cullin/F-box (SCF) E3 ubiquitin ligase pathway, specifically interacting with the SCF^{Cdc4} and SCF^{Grr1} complexes in yeast.[36,41,43,49,50] Moreover, Sgt1 has been found to be implicated in the adenylyl cyclase pathway in yeast and the innate immune systems of plants and animals.[51–55] It seems that Sgt1 prefers leucine-rich repeat (LRR)-containing proteins, putatively binding them via its SGS domain.[56,57] However, mechanistically, Sgt1 appears to have a general impact on Hsp90-dependent client maturation as its knockdown in yeast affected all clients tested.[31]

Despite its importance, the specific function and underlying mechanism of Sgt1 within the Hsp90 cycle remain unclear. Here, we set out to define the structure-function relationship of Sgt1 and elucidate its function in the Hsp90 chaperone machinery through *in vitro* and *in vivo* experiments. Our results identify a critical structural element within the SGS domain that mediates Sgt1's essential function and is directly linked to its chaperone function. We show that Sgt1 facilitates client maturation by stabilizing Hsp90-client complexes and shielding them from premature release by Aha1. Together, our findings provide mechanistic insight into how Sgt1 integrates into the Hsp90 co-chaperone network to ensure efficient client folding.

RESULTS

The SGS domain of Sgt1 is essential

Sgt1 is essential for yeast viability.[36] To define the domain(s) of Sgt1 that harbor the essential function, we performed plasmid shuffling experiments, which allowed us to express Sgt1 domain

constructs in a *sgt1Δ* knockout strain and to determine their ability to support yeast growth. As expected, the expression of full-length Sgt1 rescued the chromosomal deletion of Sgt1 (Figure 1B). However, yeast cells expressing only the TPR, the CS, or both domains were inviable. Remarkably, the expression of the SGS domain alone was sufficient to support wild-type-like growth, demonstrating that this domain harbors the essential *in vivo* function of Sgt1. Moreover, the SGS domain-containing constructs, i.e., CS-SGS or TPR-L-SGS, in which a poly-GS linker connects the TPR and SGS domains, also showed wild-type-like growth (Figure S1A). Previous work has shown that the human ortholog Sugt1 can perform the essential function of yeast Sgt1.[36] Extending this observation, we now show that both full-length human isoforms, Sugt1A and Sugt1B, as well as the human SGS domain alone, are sufficient to support growth, indicating that the essential function of the SGS domain is highly conserved from yeast to humans (Figure S1B).

While structures of the CS and TPR domains of Sgt1 are known, the conformation of the unique SGS domain is unknown and has been predicted to be primarily disordered without a globular structure.[44,45] We used NMR spectroscopy to characterize the conformation of the SGS domain. Secondary structure propensity derived from secondary ^{13}C chemical shifts identified two helical regions between amino acids 339–348 (α1) and 352–364 (α2) (Figure 1C), in agreement with an AlphaFold 2 model. The AlphaFold model of the Sgt1-SGS predicts a defined conformation for the region comprising these two α-helices and a C-terminal loop. In this part of the model, the pLDDT scores are high, indicating a high-confidence level in the local geometry. Notably, the C-terminal loop appears to engage in stabilizing interactions with the second helix, suggesting a backbinding arrangement that could help to stabilize this segment. However, backbone flexibility assessed by heteronuclear $\{^1H\}$-^{15}N NOE analysis shows that the SGS domain is overall largely flexible but that the two helical regions are more rigid, with values around 0.5, still indicating significant conformational dynamics compared with what would be expected for a rigid globular domain. Consistent with this, paramagnetic relaxation enhancement (PRE) measurements on the SGS with a spin label probe attached to residue 375 (within the C-terminal loop) show significant line broadening covering the helical regions but do not agree with theoretical PRE effects predicted for the AlphaFold model (Figure 1D). Similarly, experimentally determined residual dipolar couplings (RDCs) do not support the AlphaFold model and are consistent with significant dynamic averaging of local structural elements (Figure S1C). These results suggest that the helical regions in the SGS domain alternate between conformational states of varying compaction without making stable long-range contacts. In summary, our results revealed that the SGS domain is the essential domain of Sgt1 and that this structure is a dynamic conformational ensemble with two helical regions.

Sgt1 promotes GR maturation *in vivo* via its essential structural element

Next, we wondered whether the helical regions, which are evolutionarily conserved (Figure S1D), contribute to the essential function of the SGS domain. To test this, we introduced proline residues in the first (F343P) or the second (M358P) helix to perturb the helical conformation and performed plasmid shuffling with these variants. To show that the introduced mutations lead to breaking of the corresponding helix, we performed far UV circular dichroism (CD) spectroscopy on the purified wild-type and mutant SGS domains. These confirmed that the introduced mutations effectively disrupted the helical structure of the SGS domain (Figure S2A). Mutation of the first helix did not affect yeast cell growth, whereas breakage of the second helix was lethal, demonstrating that the essential function of Sgt1 depends on the second helix (Figure 2A). To test whether the regions adjacent to the second helix are involved in the essential function, we mutated the linker region between the two helices to alanine (349-352Ala). Yeast cells expressing only the mutated Sgt1 showed no growth defect, indicating that the linker between the two helices is not essential (Figure S2B). Truncation of the C-terminal tail revealed that a deletion up to amino acid 372 induced reduced but robust growth (Figures 2A and S2D). By contrast, a truncation up to amino acid 371 was lethal. Interestingly, the second helix ends at amino acid 364. Thus, this experiment identified the second helix plus the eight subsequent amino acids of the C-terminal tail as critical for the essential function of Sgt1 (Figure 2B). Comparison of NMR spectra from the corresponding truncated constructs lacking the TPR domain revealed a severe line broadening in CS-371 compared with CS-372, with only negligible changes in chemical shifts. This likely results from a pronounced reduction in the observable population of the helical conformation and an increase in intermediate exchange (Figures S2E and S2F), indicating the stability of the helices in the SGS as critical for Sgt1's function.

To study the chaperone function of Sgt1 *in vivo*, we used the temperature-sensitive strain *sgt1-3* (hereafter referred to as *sgt1-ts*). Since a complete knockout of Sgt1 is not viable, the ts-strain provides an alternative for studying both lethal and viable Sgt1 mutations. The *sgt1-ts* strain carries multiple mutations in the *SGT1 gene*, which cause growth defects at 25°C and 30°C and result in lethality at 37°C.[36] We transformed the *sgt1-ts* strain with plasmids, allowing the simultaneous expression of Sgt1 (full-length, domains, or mutants) along with the glucocorticoid receptor (GR) (Figure 2C). GR is a well-studied transcription factor strongly dependent on the Hsp70 and Hsp90 chaperone system for its maturation and activation.[31,58–60] At 30°C, GR levels in whole yeast extracts were severely reduced in the *sgt1-ts* strain compared with the WT (Figure 2D). Reconstitution of Sgt1 expression in the ts-strain restored GR levels to those observed in WT yeast, indicating that the stability of GR is strongly dependent on Sgt1 in yeast. Besides GR, we tested the influence of Sgt1 on another strongly Hsp90-dependent client, the oncogenic kinase v-Src. Proper folding and maturation of v-Src are lethal in wild-type yeast, making it a widely used reporter of Hsp90 function.[32,61–63] Conditional expression of v-Src in wild-type and *sgt1-ts* strains revealed that, while uninduced *sgt1-ts* cells showed reduced viability compared with the wild-type strain at 25°C, induction of v-Src inverted this pattern (Figure S2C). Under v-Src expression, *sgt1-ts* cells displayed significantly increased viability compared with the wild-type. Notably, overexpression of Sgt1 reduced the growth of the *sgt1-ts* strain to WT levels. Together, these results

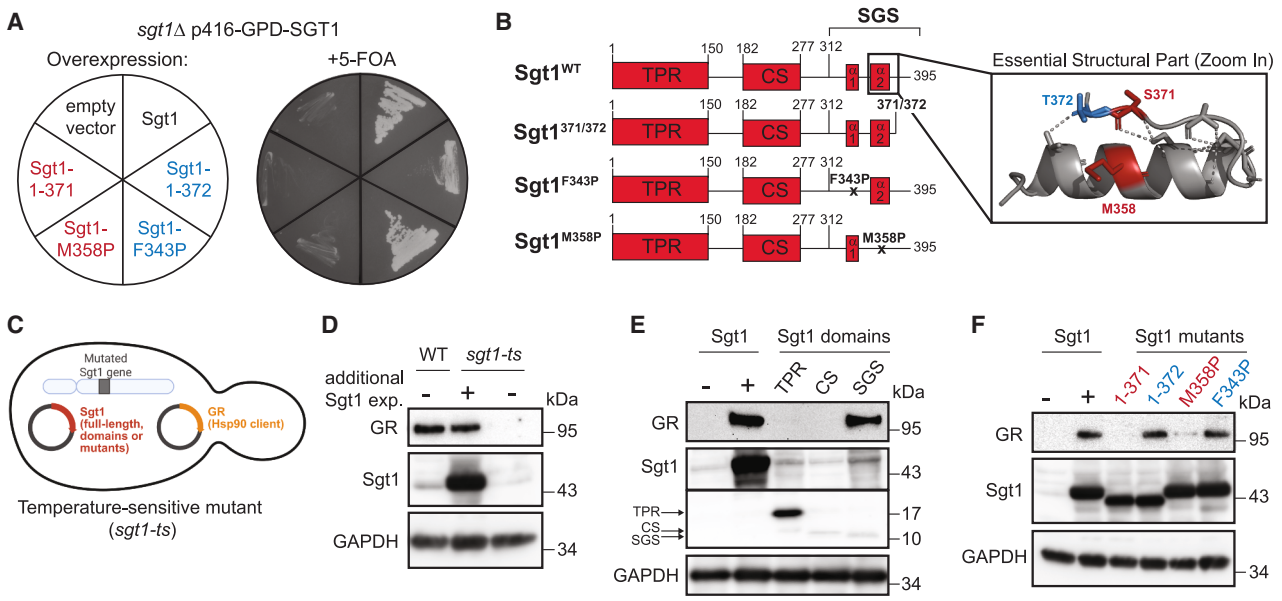

Figure 2. Sgt1 stabilizes GR *in vivo*

(A) *In vivo* analysis of the essential structural element of Sgt1. Plasmid shuffling (right) of the *sgt1Δ* p416-GPD-SGT1 strain transformed with the empty vector (p415-GPD) or plasmids overexpressing wild-type Sgt1, lethal mutants (red), or viable mutants (blue), as indicated (left). Transformants were streaked on 5-FOA plates and grown for 3 days at 30°C.

(B) Schematic domain architecture of Sgt1 truncations and point mutants, with a zoom in of the essential structural element within the AF2-predicted structure. The key residues involved in viability are highlighted.

(C) Schematic illustration of the temperature-sensitive strain *sgt1-3 (sgt1-ts)*. The strain was transformed with a plasmid overexpressing Sgt1 (full-length, domains, or mutants) along with a plasmid for expression of GR.

(D) Effect of Sgt1 on GR levels. The yeast strain BY4741 (WT) and *sgt1-ts* expressing Sgt1 (+) or empty vector (–) were grown at 30°C in selective medium. The levels of GR and Sgt1 were examined by immunoblot. GAPDH was used as a loading control. A representative immunoblot from three independent biological replicates is shown.

(E) Analysis of the essential structural element of Sgt1 required for chaperoning. *sgt1-ts* strains expressing Sgt1 (+), empty vector (–), or Sgt1 domains were analyzed as in (D). All immunoblots can be interpreted quantitatively except for the blot detecting the individual Sgt1 domains. Because a polyclonal antibody was used, which likely recognizes distinct epitopes within the separate domains, the band intensities are not directly comparable.

(F) *sgt1-ts* strains expressing Sgt1 (+), empty vector (–), or Sgt1 mutants were analyzed as in (D). Mutants lethal in the plasmid-shuffling assay are marked in red, and viable mutants are in blue.

indicate that Sgt1 is critical for the efficient maturation of the model clients v-Src and GR in yeast.

To test how the influence of Sgt1 on client maturation relates to its essential function in yeast, we determined to what extent the different structural elements of Sgt1 are involved in this process *in vivo*. To this end, we expressed the individual Sgt1 domains in the ts-strain and analyzed GR levels. Domain expression was verified by immunoblotting with a polyclonal antibody (Figure 2E). We could not detect GR when only the TPR or CS domain was expressed. However, GR accumulated to WT levels in the presence of the SGS domain. We used the *sgt1-ts* strain to further define the requirements for GR chaperoning compared with the essential function of Sgt1. We expressed Sgt1 constructs that either did not support yeast growth in the Sgt1 deletion strain (1–371 and M358P) or that could perform the essential function of Sgt1 (1–372 and F343P). The analysis of GR levels showed that the viable mutants stabilized GR while the lethal mutations did not (Figure 2F). Thus, the minimal structural element that carries out the essential function of Sgt1 is also responsible for chaperoning GR. In conclusion, these results suggest that Sgt1's function in the context of chaperoning proteins is essential *in vivo*.

Sgt1 binds Hsp90 via its CS and SGS domains

Many co-chaperones bind to Hsp90 through their TPR domains, and thus it was expected that Sgt1 would interact with Hsp90 similarly.[50] Analytical ultracentrifugation (AUC) analysis using the Atto488-labeled Sgt1-TPR (TPR*) domain confirmed previous findings[43] that the TPR domain does not interact with Hsp90, and consistently, a ΔMEEVD mutant of Hsp90 still bound Sgt1, demonstrating that the MEEVD motif is not involved in the Sgt1-Hsp90 interaction (Figure S3A). By contrast, AUC titration experiments using labeled Sgt1 (Sgt1*) and Hsp90 revealed a strong interaction with a K_D of 0.51 μM in the presence of ATP (Figure S3B). To gain further insight into the interaction of Sgt1 with Hsp90, we analyzed the interaction by NMR spectroscopy. Titrations of Sgt1-CS-SGS with isolated domains of Hsp90 confirmed the known binding site to the NTD,[45] with limited intensity reduction and chemical shift perturbations (CSPs) seen for residues 180–210 (Figures 3A and S3E). Surprisingly, the addition of unlabeled Hsp90-MD induced a drastic intensity reduction of NMR signals in the CS region of Sgt1-CS-SGS. Further NMR titrations revealed that the interaction of Sgt1-CS-SGS with Hsp90-MD is stronger than with Hsp90-NTD (Figure S3F).

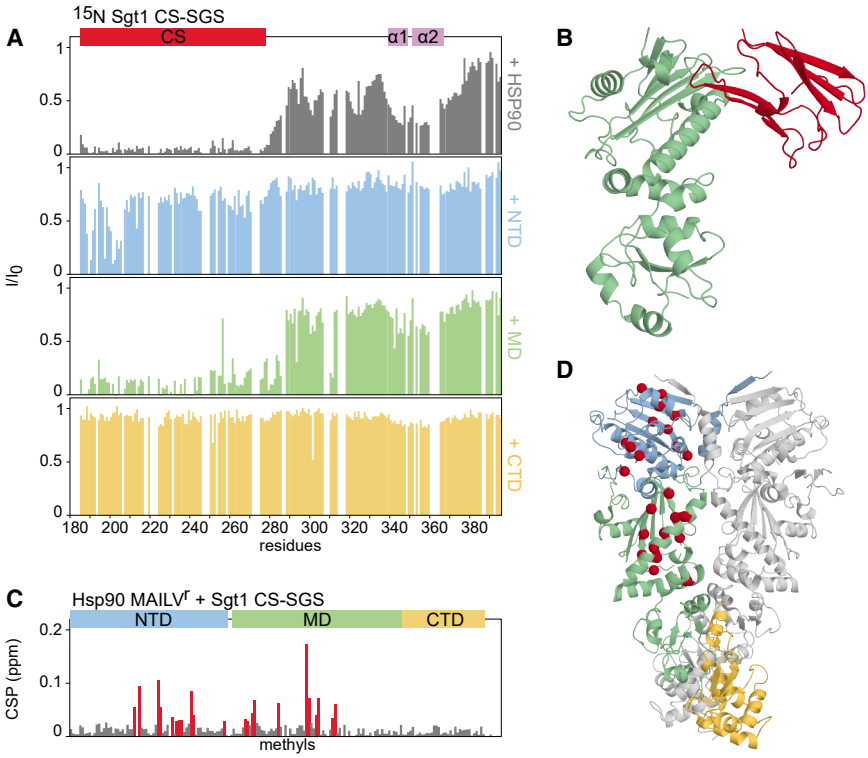

Figure 3. Sgt1-CS interacts with the NTD and MD of Hsp90

(A) NMR analysis of the interaction of Sgt1 with Hsp90 domains. The relative intensity changes of the ^{1}H-^{15}N HSQC of the Sgt1-CS-SGS before and after the addition of an equimolar amount of Hsp90-FL (gray), NTD (blue), MD (green), and CTD (yellow) show the interactions of the CS domain of Sgt1 with both NTD and MD of Hsp90.

(B) Crystal structure of the Hsp90-MD (green) and Sgt1-CS complex (red).

(C) CSP plot of ^{1}H-^{13}C TROSY of the titration on Hsp90 methyl-labeled, with Sgt1-CS-SGS, also shows both interactions in the full-length context.

(D) Structure of Hsp90 reporting methyl CSP from plot C on the structure. Residues for which CSP>0.015 are shown in red. The perturbations fit well with the known interfaces of the CS domain of Sgt1.

Consistent with this, AUC analysis confirmed that the CS domain specifically interacts with Hsp90, and experiments using labeled Sgt1 and isolated Hsp90 domains further revealed strong binding to the MD but no detectable interaction with the NTD, indicating a transient and possibly weak interaction (Figures S3C and S3D). To gain a better understanding of the Sgt1 binding site in the Hsp90-MD, we determined the crystal structure of the Sgt1-CS/Hsp90-MD complex (Figure 3B). The structure confirms the interfaces observed by NMR and shows that the CS domain binds from the edge of its β-sandwich fold to the top of the Hsp90-MD helix α2. The reverse NMR titration, looking at Hsp90-MD with the addition of Sgt1-CS, further confirms the crystal structure in solution (Figure S3G). Interestingly, we have previously identified a similar binding site on the Hsp90-MD for the Hsp90 co-chaperone NudC.[64]

To learn more about this interaction, we used full-length MAILV^{r} methyl-labeled Hsp90 with the addition of unlabeled Sgt1-CS-SGS. This titration validated the interaction observed with the isolated domains and showed that the NTD and MD binding sites are occupied in the full-length context (Figures 3C and 3D). Titration of Sgt1-CS-SGS constructs to Hsp90-MD-CTD MAILV^{r} shows the expected MD binding site with small additional chemical shift changes in the CTD compared with those seen with the Sgt1-CS construct, suggesting that the SGS region induced these (Figures S4A–S4C). In the titration of Sgt1-CS-SGS, only marginal changes of intensity are observed in the SGS region upon addition of Hsp90-CTD (Figure 3A), consistent with a weak and dynamic interaction between the SGS of Sgt1 and the CTD of Hsp90. Also, no complex is detected by AUC between Sgt1-SGS and Hsp90, confirming the weak nature of this interaction (Figure S3C). Similar transient interactions with the client-binding region of the CTD involving flexible helical regions have been previously observed with other CS-containing co-chaperones, p23 and NudC.[18,64]

We were intrigued by the apparent paradox that the CS domain is the main contributor to the interaction with Hsp90, while the SGS domain is essential for Sgt1's function. Since all constructs in the viability assays were expressed under the robust GPD promoter, we explored whether the SGS domain alone could support yeast growth using the native promoter (1,000 bp upstream of the *SGT1* gene). Interestingly, the SGS domain was insufficient to maintain yeast viability under these conditions. However, the expression of the CS-SGS construct did sustain yeast growth, indicating that the CS domain contributes an additional, albeit non-essential, function (Figure S4D). These findings suggest that the CS domain may provide a stable interaction with Hsp90, enabling the SGS domain to effectively perform its chaperone function. Altogether, our data identify a previously unknown binding site of Sgt1-CS in the Hsp90-MD. While the SGS domain exhibits a dynamic and weak interaction with the Hsp90-CTD, the interaction of Sgt1 and Hsp90 is primarily mediated by the CS domain. This raises the question of why the SGS domain is so critical for yeast viability.

Sgt1 does not interact with the Hsp70 system

Previous work showed an interaction of the SGS domain of human and plant Sgt1 with Hsp70 and thus suggested that Sgt1 may function as an adaptor protein linking the Hsp70 and Hsp90 chaperone systems.[47,48] AUC analysis with labeled Sgt1, however, did not reveal complex formation with Hsp70. NMR binding experiments with ^{15}N-labeled CS-SGS further confirmed that Hsp70 does not interact with Sgt1 (Figures S5A and S5B). To test whether Sgt1-SGS might instead interact with J-domain protein (JDP, referred to here as Hsp40) co-chaperones, as has been previously seen for the Hsp90 cofactor NudC, we tested the yeast Hsp40

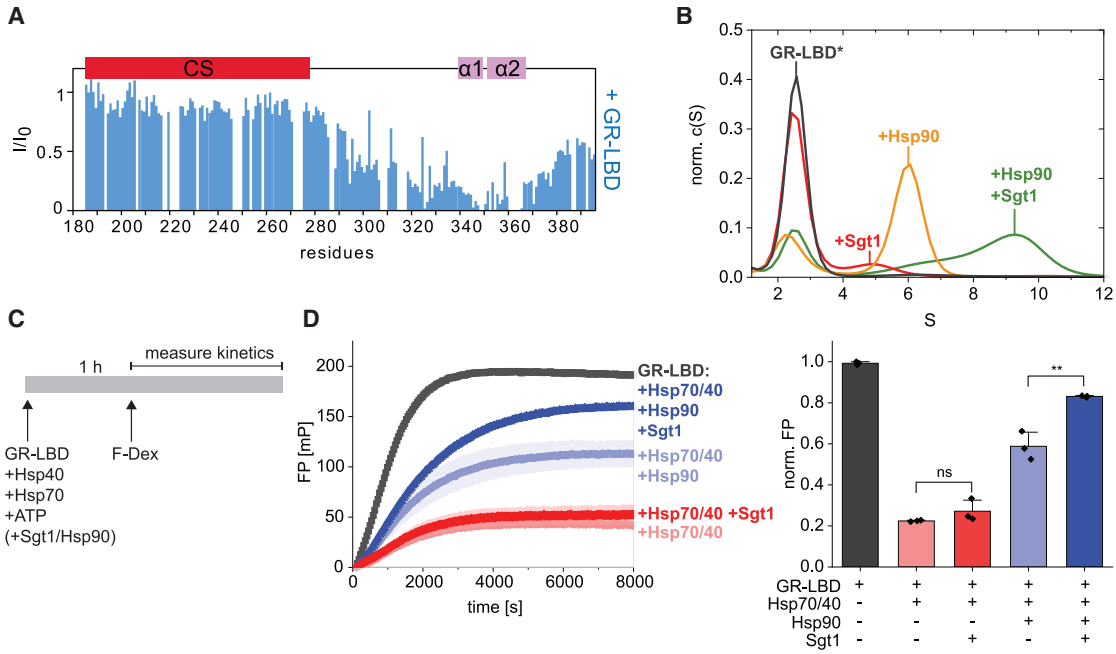

Figure 4. Sgt1 facilitates client folding *in vitro*

(A) Relative intensity changes from the ^{1}H-^{15}N HSQC of Sgt1-CS-SGS before and after the addition of GR-LBDm show that GR interacts with the SGS domain.

(B) Sgt1 forms a ternary complex with Hsp90 and GR-LBD. Complex formation analysis of labeled GR-LBD* with Sgt1 (red), Hsp90 (orange), or both (green) by AUC sedimentation is shown (GR-LBD*: 500 nM, Hsp90: 10 μM, Sgt1: 10 μM, ATP: 2 mM).

(C) Experimental setup to follow hormone binding to apo-GR-LBD. GR-LBD (1 μM) was preincubated with Hsp40 (Ydj1, 2 μM), Hsp70 (12 μM), ATP (5 mM), and chaperones Hsp90 (4 μM) and Sgt1 (12 μM) for 1 h. The reaction was initiated by the addition of fluorescein-dexamethasone (F-Dex, 100 nM).

(D) Effect of Sgt1 on Hsp90-induced hormone binding to GR-LBD. Fluorescence polarization (FP) measurement as described in (C). Left: the binding kinetics of F-Dex to GR-LBD over time are shown, with the initial millipolarization (mP) value set to zero immediately after F-Dex addition. Right: total change in fluorescence polarization was quantified and normalized to samples containing GR-LBD alone. Data are presented as mean ± SD from three independent measurements. Statistical significance was determined by a two-tailed Student's *t* test (ns $p \geq 0.05$, $^{**}p < 0.01$).

protein Ydj1. The addition of a 2-fold excess of Ydj1 to ^{15}N-labeled CS-SGS showed only a very weak binding (Figure S5A), suggesting that Sgt1 does not form a substantial interaction with Ydj1. These results strongly indicate that Sgt1 does not directly link the Hsp70 and Hsp90 chaperone systems in yeast.

Ternary complex formation by Sgt1, GR-LBD, and Hsp90 promotes client maturation efficiency

We next asked whether the SGS domain is required for interaction with client proteins, while the CS domain mediates Hsp90 binding. To test whether Sgt1 can directly interact with GR, we performed NMR analysis using the ^{15}N-labeled CS-SGS fragment together with the ligand-binding domain of GR (GR-LBD), which is targeted by chaperones within the GR.[15,19,65–67] The NMR results showed line broadening and chemical shift changes for SGS residues in the presence of the GR-LBD. Analysis of these changes suggests that the GR-LBD binds specifically to the helices within the SGS domain of Sgt1 (Figures 4A and S5C). As our results so far showed that Sgt1 can bind both GR-LBD and Hsp90, we wondered whether a ternary complex can form. To address this, we performed AUC analysis of fluorescently labeled GR-LBD (GR-LBD*). Using a labeled component greatly simplifies interpretation in multi-component mixtures,[68–70] as only the labeled protein contributes to the signal, and therefore peaks in the fluorescence trace directly reflect complexes containing the labeled protein. GR-LBD* alone sediments at 2.5S. Upon addition of Hsp90 or Sgt1, new peaks appear at 6S and 5S, respectively, consistent with binary complex formation (Figure 4B). When all three proteins were combined, a distinct peak at 9S emerged, demonstrating the formation of a ternary GR-LBD/Hsp90/Sgt1 complex (Figure 4B). Remarkably, when Sgt1 and Hsp90 were present at equimolar concentrations, the ternary complex fully replaced the GR-LBD/Hsp90 complex (Figure S5D). The additional presence of Ydj1 and Hsp70 did not influence this assembly, suggesting a remarkably high affinity of the ternary complex and supporting the conclusion that Sgt1 does not interact significantly with either component of the Hsp70 system (Figure S5E). Co-immunoprecipitation from yeast lysates confirmed that Sgt1 engages with Hsp90 and the client GR-LBD *in vivo* (Figure S5F). Overall, these results show that Sgt1 is able to form a ternary complex with GR-LBD and Hsp90 by contacting both proteins.

Next, we sought to assess the influence of Sgt1 on client maturation by the Hsp90 chaperone system. To do this, we employed a fluorescence anisotropy-based assay that monitors the hormone-binding capacity of the GR-LBD.[60,71,72] This assay takes advantage of the fact that hormone binding to the GR-LBD strongly depends on its maturation state in the folding process.

During the early folding stages, GR-LBD is bound to the Hsp70/Hsp40 system, which keeps the client in an unfolded conformation, thereby preventing hormone binding. Upon release from Hsp70 and subsequent transfer to Hsp90, the GR-LBD can proceed through the folding pathway, ultimately regaining its hormone-binding ability.[71] We incubated the GR-LBD with different combinations of the proteins Hsp70/Hsp40(Ydj1), Hsp90, and Sgt1 and monitored the binding of the fluorescently labeled hormone dexamethasone (Figure 4C). Adding Hsp70/Hsp40 to the GR-LBD significantly reduced its hormone-binding capacity. However, adding Sgt1 alone did not improve the hormone-binding capacity (Figure 4D). As expected, adding Hsp90 increased the hormone-binding capacity by around 40%. Remarkably, the simultaneous addition of Hsp90 and Sgt1 increased the hormone binding of GR-LBD by about 60%, indicating a synergistic effect of Hsp90 and Sgt1 in client maturation. Together, our results suggest that Sgt1 is not sufficient to recruit the GR-LBD from the Hsp70/Hsp40 deadlock but that the direct interaction of Sgt1 with the GR-LBD and Hsp90 facilitates the formation of a client/Sgt1/Hsp90 complex in which Sgt1 enhances client folding by Hsp90.

Sgt1 stabilizes the Hsp90-GR interaction and prevents client release by Aha1

Next, we investigated the interplay of Sgt1 with members of the Hsp90 co-chaperone system, focusing specifically on co-chaperones involved in client transfer and processing. We tested whether these co-chaperones can form complexes with Hsp90 and Sgt1. In line with previous results,[43] our AUC analysis revealed that Sti1 (hereafter referred to by the more commonly used name Hop), a key co-chaperone for client transfer, binds to both the Hsp90/Sgt1 and the GR/Hsp90/Sgt1 complexes (Figures S6A and S6B), indicating that Sgt1 adds an additional layer of regulation to the co-chaperone system. Sba1 (hereafter referred to as p23), a co-chaperone that selectively binds Hsp90 in its ATP-bound state and supports client maturation, was found to compete with Sgt1 for binding to closed Hsp90 when present in great excess (Figures S6C and S6D). Consistent with earlier studies,[43] we found that Sgt1 does not affect Hsp90's ATPase activity, even in the presence of p23 or Hop (Figure S6E).

Notably, for Aha1, a co-chaperone that accelerates the conformational cycle and binds to the MD of Hsp90,[25,34] our data indicate a distinct interaction with Sgt1. AUC experiments revealed that labeled Sgt1 and Aha1 compete for binding to Hsp90 when no client protein is present (Figure 5A). The same result was obtained using labeled Aha1 (Figure 5B). In line with the comparable binding affinities of the Hsp90-Aha1 (K_D = 0.16 to 3.8 μM[23–26,73]) and the Hsp90-Sgt1 interaction (K_D = 0.51 μM), the two co-chaperones seem to be equally capable of releasing each other (Figures 5C and 5I). Aha1 is known to bind to the NTD and MD of Hsp90. The superimposition of our structure of the Hsp90-MD/Sgt1-CS complex and the previously reported Hsp90-Aha1 structures[27] demonstrates that the two co-chaperones cannot bind simultaneously. Indeed, the CS domain of Sgt1 clashes with the binding of the Aha1-NTD to Hsp90 in both the open and closed conformations (Figure 5H).

We then investigated how the presence of a client influences this competition using labeled GR-LBD. Upon addition of Hsp90, the majority of GR-LBD is bound to Hsp90, leaving only a small fraction (~15%) unbound (Figure 5D). As seen above, the additional presence of Sgt1 leads to the uniform formation of the ternary complex consisting of GR-LBD, Hsp90, and Sgt1, completely replacing the GR-LBD/Hsp90 complex. However, Sgt1 does not further promote GR-LBD binding to Hsp90, suggesting no additional client-loading function for Sgt1. By contrast, adding Aha1 instead of Sgt1 releases the majority of GR-LBD from Hsp90, drastically increasing the proportion of free GR-LBD to nearly 80%. Previously, it was thought that Aha1 and GR-LBD were not able to bind to Hsp90 at the same time.[33] However, we can identify a peak shift of the GR-LBD/Hsp90 complex upon Aha1 addition around 1 S, indicating that while GR-LBD is mainly released from Hsp90, a complex of GR, Hsp90, and Aha1 is possible. The addition of Sgt1 to the mixture significantly inhibits the client release by Aha1, reducing it by 30% when dimeric Sgt1 and monomeric Aha1 were present at equimolar concentrations. This inhibitory effect is concentration-dependent (Figures S7A and S7B) and persists in the presence of ATP or the non-hydrolysable ATP analog ATPγS (Figure S7C). ATPase activity assays of Hsp90 mirrored these findings. The addition of Aha1 increased the Hsp90 ATPase rate by approximately 4-fold. However, this increase is lower in the presence of Sgt1, reflecting the competition of the two co-chaperones for Hsp90 binding (Figure 5E). Notably, the decreased stimulation is substantially more pronounced in the presence of client protein (GR-LBD), indicating that Sgt1 and GR-LBD synergistically stabilize the ternary complex against Aha1 (Figure 5I). To determine whether the protective effect of Sgt1 relies solely on the competition of its CS domain with Aha1 for Hsp90 binding or also involves the SGS domain, we tested an Sgt1 construct containing only the CS and TPR domains. This construct showed a reduced but still significant inhibition of both Aha1-induced client release (Figure 5F) and cycling acceleration (Figure 5G) compared with full-length Sgt1. In the absence of the client, it remained as effective as full-length Sgt1 in displacing Aha1 from Hsp90 (Figure S7D). These findings suggest that the CS and SGS domains work together to stabilize the Hsp90-client interaction and protect it from dissociation induced by Aha1, effectively prolonging the Hsp90-client interaction.

DISCUSSION

Despite its essential function in yeast, the role of Sgt1 in the Hsp90 cycle has remained elusive. Our study defines the functional mechanistic of Sgt1 and its critical structural features. Our *in vivo* analysis identified the SGS domain as critical for Sgt1's essential function. AlphaFold 2 predicts a folded region within the SGS with a relatively high pLDDT (>80) containing two helices and a constrained C-terminal loop. Our experimental NMR data confirm that the SGS encompasses two helical regions but show that the SGS is conformationally heterogeneous and does not adopt a single conformation despite the helical regions. We could pinpoint the essential function of Sgt1 to the second helical motif plus eight subsequent amino acids (up to residue 372) within the SGS domain. Interestingly, this motif is required for Sgt1's chaperone function, strongly suggesting

CellPress
OPEN ACCESS

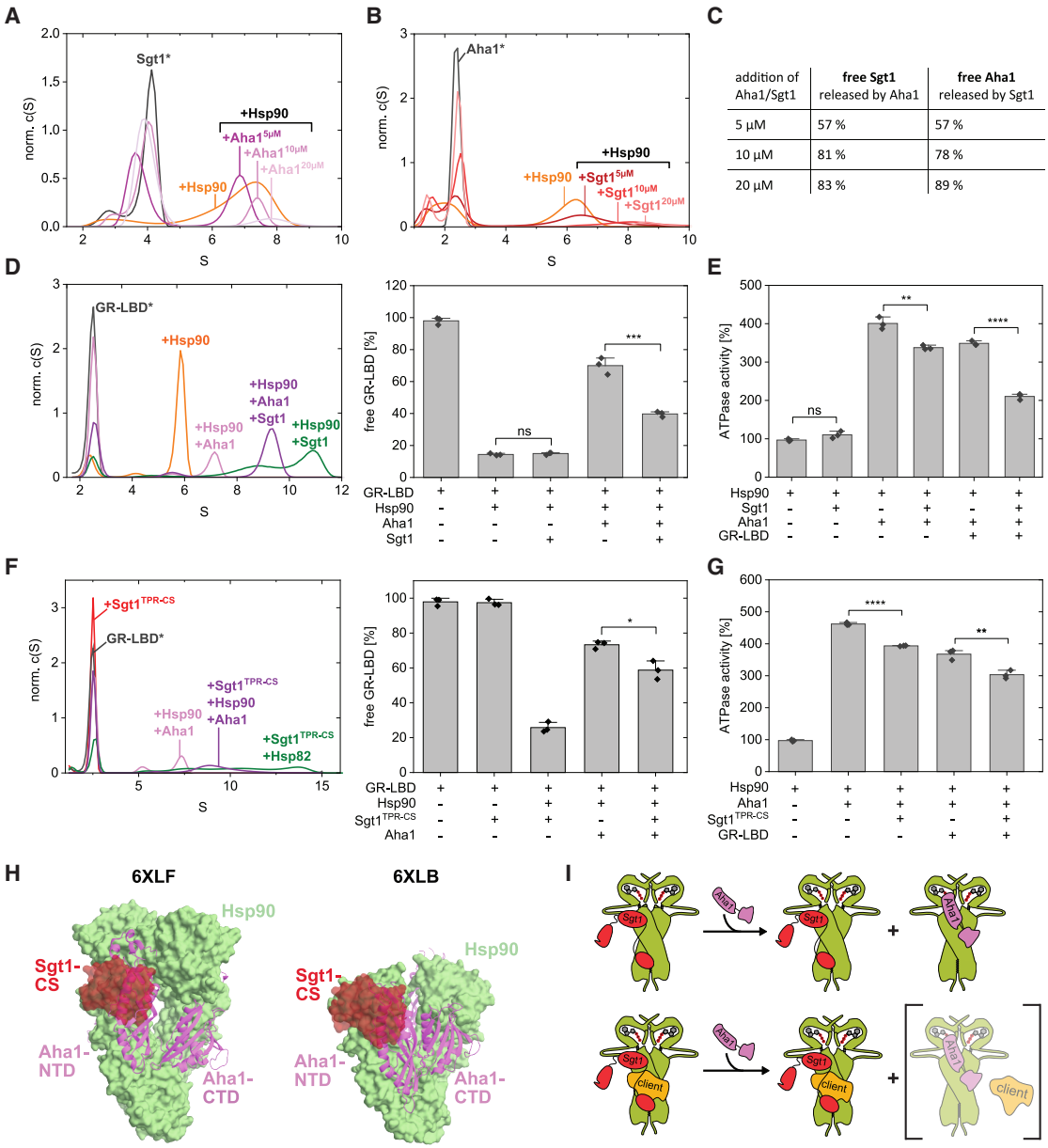

Figure 5. Sgt1 stabilizes the Hsp90-GR interaction and prevents Aha1-induced GR release from Hsp90

(A) Competition between Aha1 and Sgt1 for Hsp90 binding. Release of Sgt1 from Hsp90 by Aha1. An AUC sedimentation analysis was performed using labeled Sgt1*, Hsp90, and varying concentrations of Aha1 (Sgt1*: 500 nM, Hsp90: 5 µM, Aha1: as indicated, ATP: 5 mM).

(B) Release of Aha1 from Hsp90 by Sgt1. AUC sedimentation experiment as described in (A), but using labeled Aha1* and varying concentrations of Sgt1.

(C) Quantification of free Sgt1 and free Aha1 from panels (A) and (B) showing comparable release rates. The percentage of free Sgt1 (4 S) and free Aha1 (2.5 S) was determined by integrating the area under the respective peaks of the normalized c(S) distributions.

(D) Effect of Sgt1 on the Aha1-induced release of the GR-LBD from Hsp90. Left: representative complex formation analysis of labeled GR-LBD* in the presence of Sgt1, Hsp90, and Aha1 by AUC sedimentation is shown (GR-LBD*: 500 nM, Hsp90: 10 µM, Sgt1: 20 µM, Aha1: 10 µM, ATP: 5 mM). Right: quantification of free GR-LBD was performed by integrating the area under the free GR peak at 2.5 S. Data are presented as mean ± SD from three independent experiments. Statistical significance was determined by a two-tailed Student's *t* test (ns, $p \geq 0.05$, *$p < 0.05$, **$p < 0.01$, ***$p < 0.001$, ****$p < 0.0001$).

(E) ATPase activity of Hsp90 in the presence of Sgt1, Aha1, and GR-LBD (Hsp90: 2 µM, Aha1: 2 µM, Sgt1: 8 µM, GR-LBD: 2 µM). Results were normalized to samples containing Hsp90 alone and are shown as mean ± SD from three independent measurements. Statistical significance was determined as described in (D).

(F) AUC sedimentation experiment as described in (D), but using the Sgt1 truncation Sgt1-TPR-CS.

(G) ATPase measurement of Hsp90 as described in (E), but using the Sgt1 truncation Sgt1-TPR-CS.

(H) Superimposition of our crystal structure of the Hsp90-MD/Sgt1-CS complex on the structure of the Hsp90/Aha1 complex in its closed state (PDB: 6XLF) and open state (PDB: 6XLB) that shows that the binding sites of Aha1-NTD and Sgt1-CS overlap and are incompatible with simultaneous binding.

(I) Schematic description of the competition between Sgt1 and Aha1 for Hsp90 binding in the absence (top) and presence (bottom) of client protein.

that the chaperone function underpins its essential role. While the region is dynamic, residue S372 is predicted to create hydrogen bonding with the nearby second helix. High-confidence AlphaFold models of intrinsically disordered regions often predict their conformations in a stabilized state as adopted in the presence of partners, for example.[74] The AlphaFold model may suggest an SGS conformation when bound to partners. This conformation is likely also present in the apo SGS in low propensity but becomes too sparsely populated in the mutant CS-371, altering its function to a point where it cannot sustain yeast survival.

We found that yeast Sgt1-CS interacts with two distinct binding sites on Hsp90. The known Hsp90-NTD binding site[45] showed relatively low affinity compared with the new binding site on the Hsp90-MD. In full-length Hsp90 in the open state, both binding sites are occupied when adding Sgt1. This shows that the binding sites are not mutually exclusive. Several other Hsp90 co-chaperones feature a CS domain for Hsp90 binding, including p23 (Sba1 in yeast) and NudC in humans. The crystal structure of the Hsp90-MD and Sgt1-CS complex revealed a similar topology to that observed for NudC and Hsp90.[64] In both structures, the same interface is utilized on the MD of Hsp90; however, the CS domains of Sgt1 and NudC interact with opposite sides of their CS's β-sandwich fold. While NudC and p23 lack the SGS domain, a similar overall architecture is found, where the CS domain is followed by amphipathic helices within a largely disordered region. In both proteins, these helices have been shown to interact with clients and Hsp90.[18,19,64] Similarly, we found that the SGS domain possesses client-binding properties and is involved in transient interaction with the CTD of Hsp90. These features seem sufficient to support viability when expressed at high expression levels. However, the CS and SGS domains are essential for viability at native expression levels. This suggests that the CS-mediated interaction with Hsp90 is necessary for the SGS domain to execute its essential function. An additional client-binding function of Sgt1 has been assigned to the Sgt1-TPR domain, which binds Skp1.[36,41,43,50] While TPR domains are not exclusively dedicated to Hsp90 binding but are also employed for interactions with other partners,[75] Sgt1 is unique in that, among all known Hsp90 co-chaperones containing a TPR domain, it is the only one that does not use this module to bind Hsp90. Although Skp1 is essential in yeast, our findings suggest that its TPR interaction with Sgt1 is not essential for viability, in contrast to previous findings.[41] However, they align with the TPR domain being the least conserved domain and completely absent in several species.[76] Instead of the TPR domain, our data suggest that the interaction of the SGS domain with client proteins is essential for its function.

Previously, we found that the co-chaperone Aha1 competes with GR for binding to Hsp90.[33] Deletion of Aha1 in yeast results in increased levels of functional GR.[31] This also holds true for other proteins.[30–32] Similarly, the absence of Aha1 in mammalian cells improves the folding efficiency and stability of disease-associated CFTR.[26,29] Our results show that Sgt1 counteracts this process by effectively impairing Aha1 binding and inhibiting Aha1-induced client release. While Sgt1 is competing with Aha1 for Hsp90 interaction in the absence of the client, it seems that Sgt1 and the client protein are synergistic in blocking Aha1, probably mediated by the stabilizing effect of the SGS domain. Our results thus suggest that the two co-chaperones target later steps in the Hsp90 chaperone cycle but with opposing effects. Supporting this notion, overexpression of Aha1 in a temperature-sensitive Sgt1 mutant led to a substantial growth defect in yeast cells. This effect was abolished when an Aha1 mutant insufficient to bind to Hsp90 was used.[77] Thus, Sgt1 appears to keep the client release effect of Aha1 at bay. In the absence of Sgt1, Aha1 will reduce the dwell time of GR. Thus, Sgt1 stabilizes the Hsp90-client complex and extends the processing phase of Hsp90 for clients by shielding them from Aha1 (Figure 6).

When viewed in the broader Hsp90 co-chaperone network context, Sgt1 exhibits a distinct mechanism compared with canonical co-chaperones such as Hop and p23. Hop primarily acts early in the Hsp90 cycle by mediating client transfer from the Hsp70/Hsp40 system.[13,15] By contrast, Sgt1 does not form substantial contacts to Hsp70 or J-domain proteins and does not promote GR loading onto Hsp90, arguing against a role in client transfer. Instead, we found that Sgt1 enhances GR maturation and stabilizes Hsp90/GR complexes, pointing to a role in later stages of the chaperone cycle. However, we and others[43] observed that Hop and Sgt1 bind Hsp90 simultaneously and that Sgt1 can associate with all nucleotide states of Hsp90, suggesting that Sgt1 may be present during client loading without interfering with early steps of the cycle. Similar to Sgt1, p23 also contributes to client stabilization, binding both Hsp90 and clients while promoting the closed conformation of Hsp90.[19,21] Sgt1 differs, however, in that it engages with all states of Hsp90 and does not influence its enzymatic activity,[43] highlighting a distinct mechanism. We observed that high concentrations of p23 can displace Sgt1 from closed Hsp90, a finding consistent with observations for nematode Sgt1,[76] suggesting a degree of competition or sequential binding. While Sgt1 clearly blocks Aha1 access and associated client release, it remains to be tested whether p23 has a similar protective function.

Sgt1 is highly conserved across eukaryotes, raising the question of whether its mechanism of modulating Hsp90 is similarly conserved. A key point supporting this idea is the strong evolutionary conservation of the CS and SGS domains—both critical for Sgt1's co-chaperone function—compared with the more variable TPR domain.[76] Consistent with this, we found that the human SGS domain can functionally substitute for its yeast counterpart, underscoring a conserved role. While our experiments mainly focus on GR as a model client, previous studies have shown that the SGS domain also mediates interactions with other clients, particularly LRR-containing proteins.[56,57] These interactions appear to be SGS-dependent and conserved, suggesting that the stabilizing mechanism we describe here may extend to other client classes with similar binding requirements. The core Sgt1-Hsp90 interaction is conserved across species, although the precise binding interface has diverged. In yeast, Sgt1 primarily interacts with the MD of Hsp90, while in plants, it engages the NTD.[45] The interface in metazoans remains unresolved, and it is currently unclear whether it follows the yeast or plant binding mode, or represents a distinct, species-specific

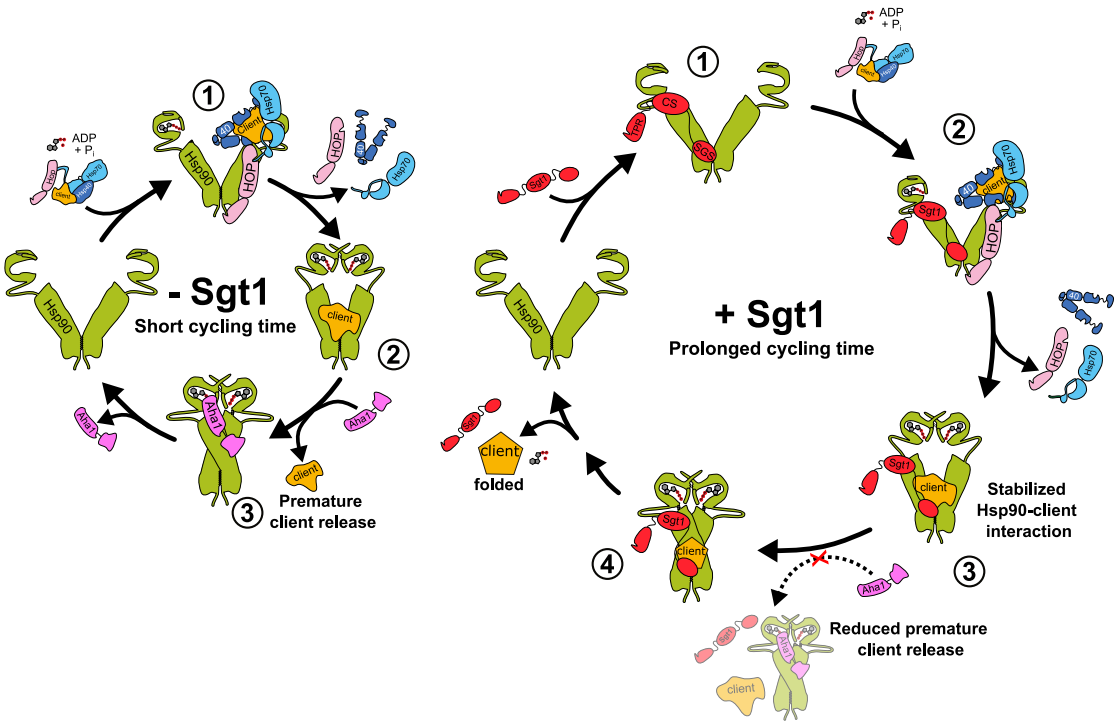

Figure 6. Schematic model of how Sgt1 influences the client maturation process

A schematic representation of Sgt1's role in the yeast Hsp90 cycle is shown. For clarity, yeast Sgt1 is depicted as a monomer, although it is capable of forming dimers. Left: in the absence of Sgt1, client proteins are transferred from the Hsp70/Hsp40 complex to Hsp90 with the help of Hop (steps 1–2). The co-chaperone Aha1 can bind to Hsp90 without restriction, accelerating the Hsp90 cycling time and promoting premature release of clients (step 3). Right: in the presence of Sgt1, client proteins are loaded onto Hsp90 via Hop (steps 1 and 2), as in the canonical cycle. However, Sgt1 stabilizes the Hsp90-client interaction and prevents excessive Aha1 binding (step 3). This slows the Hsp90 cycling time as indicated by a larger cycle and increases the dwell time of clients in the Hsp90 complex. Thus, Sgt1 promotes the proper maturation of the client protein (step 4).

interaction. Given the high degree of conservation in the Hsp90 system, including Aha1, it is possible that Sgt1-Aha1 competition is also preserved in higher eukaryotes. However, the lack of structural data on Sgt1/Hsp90 and Aha1/Hsp90 complexes in metazoans makes conservation of this competitive mechanism speculative.

In summary, our study defines the mechanistic role of Sgt1 as a late-acting co-chaperone that stabilizes Hsp90-client complexes through its CS and SGS domains. Sgt1 does not promote client loading but supports client maturation by extending dwell time on Hsp90 and counteracting Aha1-mediated client release.

Limitations of the study

While our study provides important insights into the structural and functional role of Sgt1, several limitations remain. First, we focused nearly exclusively on yeast Sgt1, and further studies are needed to determine whether homologs in other organisms, such as humans, function similarly. Second, a more detailed structural analysis of the Sgt1 interaction with the client GR-LBD and the ternary complex with Hsp90 could provide deeper insights into its structure-function relationship. Finally, whether the mechanisms described here extend to other clients of Sgt1 remains to be determined.

RESOURCE AVAILABILITY

Lead contact

Further information and requests for resources and reagents should be directed to and will be fulfilled by the lead contact, Johannes Buchner (johannes.buchner@tum.de).

Materials availability

Plasmids and yeast strains generated in this study will be made available on request, but we may require a payment and/or a completed materials transfer agreement if there is potential for commercial application.

Data and code availability

- The crystal structure of the Hsp82-MD/Sgt1-CS complex has been deposited in the Protein Data Bank and is publicly available as of the date of publication. The backbone resonance assignment of Sgt1-CS-SGS has been deposited to the Biological Magnetic Resonance Data Bank and is publicly available as of the date of publication. Accession numbers are listed in the key resources table.
- This paper does not report original code.
- Any additional information required to reanalyze the data reported in this paper is available from the lead contact upon request.

ACKNOWLEDGMENTS

We thank Kaya Bergmann for laboratory support, and we are particularly grateful to Sam Asami and Gerd Gemmecker (TUM) for support with NMR

experiments. We acknowledge access to NMR measurement time at the Bavarian NMR Center. This study was supported by the German Research Foundation DFG (SFB1035, Projektnummer 201302640, project A03). A.E. acknowledges a doctoral fellowship from the Ernst Ludwig Ehrlich Studienwerk, and S.E. acknowledges a doctoral fellowship from the Studienstiftung des Deutschen Volkes.

AUTHOR CONTRIBUTIONS

Conceptualization, F.D., S.E., C.D., A.L., J.B., and M.S.; methodology, S.E., F.D., C.D., and A.L.; investigation, F.D., S.E., C.D., A.E., A.L., V.N., G.M.P., and O.F.; visualization, S.E., F.D., and O.F.; writing – original draft, S.E. and F.D.; writing – review & editing, J.B., R.R., M.S., and O.F.; supervision, J.B., M.S., and R.R.; resources and funding acquisition, J.B., M.S., and R.R.

DECLARATION OF INTERESTS

The authors declare no competing interests.

STAR★METHODS

Detailed methods are provided in the online version of this paper and include the following:

- KEY RESOURCES TABLE
- EXPERIMENTAL MODEL AND STUDY PARTICIPANT DETAILS
  - Yeast strains
- METHOD DETAILS
  - Yeast transformation
  - Yeast viability assay
  - Plasmid shuffling
  - v-Src activity assay
  - GR stability analysis
  - Co-immunoprecipitation
  - Protein expression, purification, and labeling
  - Analytical ultracentrifugation
  - Fluorescence polarization measurement
  - ATPase assay
  - Western blot
  - Circular dichroism spectroscopy
  - NMR
  - Chemical shift assignments
  - Paramagnetic relaxation enhancements (PRE)
  - Residual dipolar couplings
  - Titrations
  - Crystallography
- QUANTIFICATION AND STATISTICAL ANALYSIS

SUPPLEMENTAL INFORMATION

Supplemental information can be found online at https://doi.org/10.1016/j.molcel.2025.12.002.

Received: April 11, 2025
Revised: September 23, 2025
Accepted: December 1, 2025
Published: December 22, 2025

REFERENCES

1. Balchin, D., Hayer-Hartl, M., and Hartl, F.U. (2016). In vivo aspects of protein folding and quality control. Science *353*, aac4354. https://doi.org/10.1126/science.aac4354.
2. Taipale, M., Krykbaeva, I., Koeva, M., Kayatekin, C., Westover, K.D., Karras, G.I., and Lindquist, S. (2012). Quantitative Analysis of Hsp90-Client Interactions Reveals Principles of Substrate Recognition. Cell *150*, 987–1001. https://doi.org/10.1016/j.cell.2012.06.047.
3. Zhao, R., Davey, M., Hsu, Y.-C., Kaplanek, P., Tong, A., Parsons, A.B., Krogan, N., Cagney, G., Mai, D., Greenblatt, J., et al. (2005). Navigating the Chaperone Network: An Integrative Map of Physical and Genetic Interactions Mediated by the Hsp90 Chaperone. Cell *120*, 715–727. https://doi.org/10.1016/j.cell.2004.12.024.
4. Schopf, F.H., Biebl, M.M., and Buchner, J. (2017). The HSP90 chaperone machinery. Nat. Rev. Mol. Cell Biol. *18*, 345–360. https://doi.org/10.1038/nrm.2017.20.
5. Taipale, M., Jarosz, D.F., and Lindquist, S. (2010). HSP90 at the hub of protein homeostasis: emerging mechanistic insights. Nat. Rev. Mol. Cell Biol. *11*, 515–528. https://doi.org/10.1038/nrm2918.
6. Minami, Y., Kimura, Y., Kawasaki, H., Suzuki, K., and Yahara, I. (1994). The carboxy-terminal region of mammalian HSP90 is required for its dimerization and function in vivo. Mol. Cell. Biol. *14*, 1459–1464. https://doi.org/10.1128/mcb.14.2.1459-1464.1994.
7. Prodromou, C., Panaretou, B., Chohan, S., Siligardi, G., O'Brien, R., Ladbury, J.E., Roe, S.M., Piper, P.W., and Pearl, L.H. (2000). The ATPase cycle of Hsp90 drives a molecular clamp' via transient dimerization of the N-terminal domains. EMBO J. *19*, 4383–4392. https://doi.org/10.1093/emboj/19.16.4383.
8. Hessling, M., Richter, K., and Buchner, J. (2009). Dissection of the ATP-induced conformational cycle of the molecular chaperone Hsp90. Nat. Struct. Mol. Biol. *16*, 287–293. https://doi.org/10.1038/nsmb.1565.
9. Prodromou, C., Roe, S.M., O'Brien, R., Ladbury, J.E., Piper, P.W., and Pearl, L.H. (1997). Identification and Structural Characterization of the ATP/ADP-Binding Site in the Hsp90 Molecular Chaperone. Cell *90*, 65–75. https://doi.org/10.1016/S0092-8674(00)80314-1.
10. Johnson, J.L. (2012). Evolution and function of diverse Hsp90 homologs and cochaperone proteins. BBA Mol. Cell Res. *1823*, 607–613. https://doi.org/10.1016/j.bbamcr.2011.09.020.
11. Biebl, M.M., and Buchner, J. (2019). Structure, Function, and Regulation of the Hsp90 Machinery. Cold Spring Harb. Perspect. Biol. *11*, a034017. https://doi.org/10.1101/cshperspect.a034017.
12. Engler, S., and Buchner, J. (2025). The evolution and diversification of the Hsp90 co-chaperone system. Biol. Chem. *406*, 309–329. https://doi.org/10.1515/hsz-2025-0112.
13. Chen, S., and Smith, D.F. (1998). Hop as an Adaptor in the Heat Shock Protein 70 (Hsp70) and Hsp90 Chaperone Machinery. J. Biol. Chem. *273*, 35194–35200. https://doi.org/10.1074/jbc.273.52.35194.
14. Johnson, B.D., Schumacher, R.J., Ross, E.D., and Toft, D.O. (1998). Hop Modulates hsp70/hsp90 Interactions in Protein Folding. J. Biol. Chem. *273*, 3679–3686. https://doi.org/10.1074/jbc.273.6.3679.
15. Wang, R.Y.-R., Noddings, C.M., Kirschke, E., Myasnikov, A.G., Johnson, J.L., and Agard, D.A. (2022). Structure of Hsp90-Hsp70-Hop-GR reveals the Hsp90 client-loading mechanism. Nature *601*, 460–464. https://doi.org/10.1038/s41586-021-04252-1.
16. Dittmar, K.D., Demady, D.R., Stancato, L.F., Krishna, P., and Pratt, W.B. (1997). Folding of the glucocorticoid receptor by the heat shock protein (hsp) 90-based chaperone machinery. The role of p23 is to stabilize receptor.hsp90 heterocomplexes formed by hsp90.p60.hsp70. J. Biol. Chem. *272*, 21213–21220. https://doi.org/10.1074/jbc.272.34.21213.
17. Freeman, B.C., Felts, S.J., Toft, D.O., and Yamamoto, K.R. (2000). The p23 molecular chaperones act at a late step in intracellular receptor action to differentially affect ligand efficacies. Genes Dev. *14*, 422–434. https://doi.org/10.1101/gad.14.4.422.
18. Biebl, M.M., Lopez, A., Rehn, A., Freiburger, L., Lawatscheck, J., Blank, B., Sattler, M., and Buchner, J. (2021). Structural elements in the flexible tail of the co-chaperone p23 coordinate client binding and progression of the Hsp90 chaperone cycle. Nat. Commun. *12*, 828. https://doi.org/10.1038/s41467-021-21063-0.

19. Noddings, C.M., Wang, R.Y.-R., Johnson, J.L., and Agard, D.A. (2022). Structure of Hsp90-p23-GR reveals the Hsp90 client-remodelling mechanism. Nature *601*, 465–469. https://doi.org/10.1038/s41586-021-04236-1.

20. Ali, M.M.U., Roe, S.M., Vaughan, C.K., Meyer, P., Panaretou, B., Piper, P.W., Prodromou, C., and Pearl, L.H. (2006). Crystal structure of an Hsp90-nucleotide-p23/Sba1 closed chaperone complex. Nature *440*, 1013–1017. https://doi.org/10.1038/nature04716.

21. Richter, K., Walter, S., and Buchner, J. (2004). The Co-chaperone Sba1 Connects the ATPase Reaction of Hsp90 to the Progression of the Chaperone Cycle. J. Mol. Biol. *342*, 1403–1413. https://doi.org/10.1016/j.jmb.2004.07.064.

22. Karagöz, G.E., Duarte, A.M.S., Ippel, H., Uetrecht, C., Sinnige, T., van Rosmalen, M., Hausmann, J., Heck, A.J.R., Boelens, R., and Rüdiger, S.G.D. (2011). N-terminal domain of human Hsp90 triggers binding to the cochaperone p23. Proc. Natl. Acad. Sci. USA. *108*, 580–585. https://doi.org/10.1073/pnas.1011867108.

23. Meyer, P., Prodromou, C., Liao, C., Hu, B., Mark Roe, S., Vaughan, C.K., Vlasic, I., Panaretou, B., Piper, P.W., and Pearl, L.H. (2004). Structural basis for recruitment of the ATPase activator Aha1 to the Hsp90 chaperone machinery. EMBO J. *23*, 511–519. https://doi.org/10.1038/sj.emboj.7600060.

24. Retzlaff, M., Hagn, F., Mitschke, L., Hessling, M., Gugel, F., Kessler, H., Richter, K., and Buchner, J. (2010). Asymmetric activation of the hsp90 dimer by its cochaperone aha1. Mol. Cell *37*, 344–354. https://doi.org/10.1016/j.molcel.2010.01.006.

25. Panaretou, B., Siligardi, G., Meyer, P., Maloney, A., Sullivan, J.K., Singh, S., Millson, S.H., Clarke, P.A., Naaby-Hansen, S., Stein, R., et al. (2002). Activation of the ATPase Activity of Hsp90 by the Stress-Regulated Cochaperone Aha1. Mol. Cell *10*, 1307–1318. https://doi.org/10.1016/S1097-2765(02)00785-2.

26. Koulov, A.V., LaPointe, P., Lu, B., Razvi, A., Coppinger, J., Dong, M.-Q., Matteson, J., Laister, R., Arrowsmith, C., Yates, J.R., et al. (2010). Biological and structural basis for Aha1 regulation of Hsp90 ATPase activity in maintaining proteostasis in the human disease cystic fibrosis. Mol. Biol. Cell *21*, 871–884. https://doi.org/10.1091/mbc.e09-12-1017.

27. Liu, Y., Sun, M., Myasnikov, A.G., Elnatan, D., Delaeter, N., Nguyenquang, M., and Agard, D.A. (2020). Cryo-EM structures reveal a multistep mechanism of Hsp90 activation by co-chaperone Aha1. bioRxiv. https://doi.org/10.1101/2020.06.30.180695.

28. Lotz, G.P., Lin, H., Harst, A., and Obermann, W.M.J. (2003). Aha1 Binds to the Middle Domain of Hsp90, Contributes to Client Protein Activation, and Stimulates the ATPase Activity of the Molecular Chaperone. J. Biol. Chem. *278*, 17228–17235. https://doi.org/10.1074/jbc.M212761200.

29. Wang, X., Venable, J., LaPointe, P., Hutt, D.M., Koulov, A.V., Coppinger, J., Gurkan, C., Kellner, W., Matteson, J., Plutner, H., et al. (2006). Hsp90 cochaperone Aha1 downregulation rescues misfolding of CFTR in cystic fibrosis. Cell *127*, 803–815. https://doi.org/10.1016/j.cell.2006.09.043.

30. Ran, F., Gadura, N., and Michels, C.A. (2010). Hsp90 cochaperone Aha1 is a negative regulator of the Saccharomyces MAL activator and acts early in the chaperone activation pathway. J. Biol. Chem. *285*, 13850–13862. https://doi.org/10.1074/jbc.M109.040600.

31. Sahasrabudhe, P., Rohrberg, J., Biebl, M.M., Rutz, D.A., and Buchner, J. (2017). The Plasticity of the Hsp90 Co-chaperone System. Mol. Cell *67*, 947–961.e5. https://doi.org/10.1016/j.molcel.2017.08.004.

32. Biebl, M.M., Riedl, M., and Buchner, J. (2020). Hsp90 Co-chaperones Form Plastic Genetic Networks Adapted to Client Maturation. Cell Rep. *32*, 108063. https://doi.org/10.1016/j.celrep.2020.108063.

33. Lorenz, O.R., Freiburger, L., Rutz, D.A., Krause, M., Zierer, B.K., Alvira, S., Cuéllar, J., Valpuesta, J.M., Madl, T., Sattler, M., et al. (2014). Modulation of the Hsp90 Chaperone Cycle by a Stringent Client Protein. Mol. Cell *53*, 941–953. https://doi.org/10.1016/j.molcel.2014.02.003.

34. Meyer, P., Prodromou, C., Hu, B., Vaughan, C., Roe, S.M., Panaretou, B., Piper, P.W., and Pearl, L.H. (2003). Structural and functional analysis of the middle segment of hsp90: implications for ATP hydrolysis and client protein and cochaperone interactions. Mol. Cell *11*, 647–658. https://doi.org/10.1016/S1097-2765(03)00065-0.

35. Biebl, M.M., and Buchner, J. (2023). p23 and Aha1: Distinct Functions Promote Client Maturation. Subcell. Biochem. *101*, 159–187. https://doi.org/10.1007/978-3-031-14740-1_6.

36. Kitagawa, K., Skowyra, D., Elledge, S.J., Harper, J.W., and Hieter, P. (1999). SGT1 encodes an essential component of the yeast kinetochore assembly pathway and a novel subunit of the SCF ubiquitin ligase complex. Mol. Cell *4*, 21–33. https://doi.org/10.1016/s1097-2765(00)80184-7.

37. Niikura, Y., and Kitagawa, K. (2003). Identification of a novel splice variant: human SGT1B (SUGT1B). DNA Seq. *14*, 436–441. https://doi.org/10.1080/10425170310001623644.

38. Zou, X., Ji, C., Wang, L., Wu, M., Zheng, H., Xu, J., Jin, F., Gu, S., Ying, K., Xie, Y., et al. (2004). Molecular cloning and characterization of SGT1.2, a novel splice variant of Homo sapiens SGT1. DNA Seq. *15*, 140–143. https://doi.org/10.1080/10425170320000160215.

39. Zabka, M., Leśniak, W., Prus, W., Kuźnicki, J., and Filipek, A. (2008). Sgt1 has co-chaperone properties and is up-regulated by heat shock. Biochem. Biophys. Res. Commun. *370*, 179–183. https://doi.org/10.1016/j.bbrc.2008.03.055.

40. Bansal, P.K., Nourse, A., Abdulle, R., and Kitagawa, K. (2009). Sgt1 Dimerization Is Required for Yeast Kinetochore Assembly. J. Biol. Chem. *284*, 3586–3592. https://doi.org/10.1074/jbc.M806281200.

41. Willhoft, O., Kerr, R., Patel, D., Zhang, W., Al-Jassar, C., Daviter, T., Millson, S.H., Thalassinos, K., and Vaughan, C.K. (2017). The crystal structure of the Sgt1-Skp1 complex: the link between Hsp90 and both SCF E3 ubiquitin ligases and kinetochores. Sci. Rep. *7*, 41626. https://doi.org/10.1038/srep41626.

42. Schmid, A.B., Lagleder, S., Gräwert, M.A., Röhl, A., Hagn, F., Wandinger, S.K., Cox, M.B., Demmer, O., Richter, K., Groll, M., et al. (2012). The architecture of functional modules in the Hsp90 co-chaperone Sti1/Hop. EMBO J. *31*, 1506–1517. https://doi.org/10.1038/emboj.2011.472.

43. Catlett, M.G., and Kaplan, K.B. (2006). Sgt1p Is a Unique Co-chaperone That Acts as a Client Adaptor to Link Hsp90 to Skp1p. J. Biol. Chem. *281*, 33739–33748. https://doi.org/10.1074/jbc.M603847200.

44. Lee, Y.-T., Jacob, J., Michowski, W., Nowotny, M., Kuznicki, J., and Chazin, W.J. (2004). Human Sgt1 Binds HSP90 through the CHORD-Sgt1 Domain and Not the Tetratricopeptide Repeat Domain. J. Biol. Chem. *279*, 16511–16517. https://doi.org/10.1074/jbc.M400215200.

45. Zhang, M., Botër, M., Li, K., Kadota, Y., Panaretou, B., Prodromou, C., Shirasu, K., and Pearl, L.H. (2008). Structural and functional coupling of Hsp90- and Sgt1-centred multi-protein complexes. EMBO J. *27*, 2789–2798. https://doi.org/10.1038/emboj.2008.190.

46. Góral, A., Bieganowski, P., Prus, W., Krzemień-Ojak, Ł., Kądziołka, B., Fabczak, H., and Filipek, A. (2016). Calcyclin Binding Protein/Siah-1 Interacting Protein Is a Hsp90 Binding Chaperone. PLoS One *11*, e0156507. https://doi.org/10.1371/journal.pone.0156507.

47. Noël, L.D., Cagna, G., Stuttmann, J., Wirthmüller, L., Betsuyaku, S., Witte, C.-P., Bhat, R., Pochon, N., Colby, T., and Parker, J.E. (2007). Interaction between SGT1 and cytosolic/nuclear HSC70 chaperones regulates Arabidopsis immune responses. Plant Cell *19*, 4061–4076. https://doi.org/10.1105/tpc.107.051896.

48. Spiechowicz, M., Zylicz, A., Bieganowski, P., Kuznicki, J., and Filipek, A. (2007). Hsp70 is a new target of Sgt1–an interaction modulated by S100A6. Biochem. Biophys. Res. Commun. *357*, 1148–1153. https://doi.org/10.1016/j.bbrc.2007.04.073.

49. Steensgaard, P., Garrè, M., Muradore, I., Transidico, P., Nigg, E.A., Kitagawa, K., Earnshaw, W.C., Faretta, M., and Musacchio, A. (2004). Sgt1 is required for human kinetochore assembly. EMBO Rep. *5*, 626–631. https://doi.org/10.1038/sj.embor.7400154.

50. Bansal, P.K., Abdulle, R., and Kitagawa, K. (2004). Sgt1 associates with Hsp90: an initial step of assembly of the core kinetochore complex. Mol.

Cell. Biol. *24*, 8069–8079. https://doi.org/10.1128/MCB.24.18.8069-8079.2004.

51. Mayor, A., Martinon, F., de De Smedt, T., Pétrilli, V., and Tschopp, J. (2007). A crucial function of SGT1 and HSP90 in inflammasome activity links mammalian and plant innate immune responses. Nat. Immunol. *8*, 497–503. https://doi.org/10.1038/ni1459.

52. Da Silva Correia, J., Miranda, Y., Leonard, N., and Ulevitch, R. (2007). SGT1 is essential for Nod1 activation. Proc. Natl. Acad. Sci. USA. *104*, 6764–6769. https://doi.org/10.1073/pnas.0610926104.

53. Shirasu, K. (2009). The HSP90-SGT1 chaperone complex for NLR immune sensors. Annu. Rev. Plant Biol. *60*, 139–164. https://doi.org/10.1146/annurev.arplant.59.032607.092906.

54. Kadota, Y., Shirasu, K., and Guerois, R. (2010). NLR sensors meet at the SGT1-HSP90 crossroad. Trends Biochem. Sci. *35*, 199–207. https://doi.org/10.1016/j.tibs.2009.12.005.

55. Dubacq, C., Guerois, R., Courbeyrette, R., Kitagawa, K., and Mann, C. (2002). Sgt1p contributes to cyclic AMP pathway activity and physically interacts with the adenylyl cyclase Cyr1p/Cdc35p in budding yeast. Eukaryot. Cell *1*, 568–582. https://doi.org/10.1128/EC.1.4.568-582.2002.

56. Taipale, M., Tucker, G., Peng, J., Krykbaeva, I., Lin, Z.-Y., Larsen, B., Choi, H., Berger, B., Gingras, A.-C., and Lindquist, S. (2014). A quantitative chaperone interaction network reveals the architecture of cellular protein homeostasis pathways. Cell *158*, 434–448. https://doi.org/10.1016/j.cell.2014.05.039.

57. Stuttmann, J., Parker, J.E., and Noël, L.D. (2008). Staying in the fold: The SGT1/chaperone machinery in maintenance and evolution of leucine-rich repeat proteins. Plant Signal. Behav. *3*, 283–285. https://doi.org/10.4161/psb.3.5.5576.

58. Pratt, W.B., Scherrer, L.C., Hutchison, K.A., and Dalman, F.C. (1992). A model of glucocorticoid receptor unfolding and stabilization by a heat shock protein complex. J. Steroid Biochem. Mol. Biol. *41*, 223–229. https://doi.org/10.1016/0960-0760(92)90348-m.

59. Pratt, W.B., Morishima, Y., Murphy, M., and Harrell, M. (2006). Chaperoning of glucocorticoid receptors. Handb. Exp. Pharmacol. *172*, 111–138. https://doi.org/10.1007/3-540-29717-0_5.

60. Kirschke, E., Goswami, D., Southworth, D., Griffin, P.R., and Agard, D.A. (2014). Glucocorticoid receptor function regulated by coordinated action of the Hsp90 and Hsp70 chaperone cycles. Cell *157*, 1685–1697. https://doi.org/10.1016/j.cell.2014.04.038.

61. Kornbluth, S., Jove, R., and Hanafusa, H. (1987). Characterization of avian and viral p60src proteins expressed in yeast. Proc. Natl. Acad. Sci. USA. *84*, 4455–4459. https://doi.org/10.1073/pnas.84.13.4455.

62. Dey, B., Lightbody, J.J., and Boschelli, F. (1996). CDC37 is required for p60v-src activity in yeast. Mol. Biol. Cell *7*, 1405–1417. https://doi.org/10.1091/mbc.7.9.1405.

63. Goeckeler, J.L., Stephens, A., Lee, P., Caplan, A.J., and Brodsky, J.L. (2002). Overexpression of yeast Hsp110 homolog Sse1p suppresses ydj1-151 thermosensitivity and restores Hsp90-dependent activity. Mol. Biol. Cell *13*, 2760–2770. https://doi.org/10.1091/mbc.02-04-0051.

64. Biebl, M.M., Delhommel, F., Faust, O., Zak, K.M., Agam, G., Guo, X., Mühlhofer, M., Dahiya, V., Hillebrand, D., Popowicz, G.M., et al. (2022). NudC guides client transfer between the Hsp40/70 and Hsp90 chaperone systems. Mol. Cell *82*, 555–569.e7. https://doi.org/10.1016/j.molcel.2021.12.031.

65. Howard, K.J., Holley, S.J., Yamamoto, K.R., and Distelhorst, C.W. (1990). Mapping the HSP90 binding region of the glucocorticoid receptor. J. Biol. Chem. *265*, 11928–11935. https://doi.org/10.1016/S0021-9258(19)38489-3.

66. Noddings, C.M., Johnson, J.L., and Agard, D.A. (2023). Cryo-EM reveals how Hsp90 and FKBP immunophilins co-regulate the glucocorticoid receptor. Nat. Struct. Mol. Biol. *30*, 1867–1877. https://doi.org/10.1038/s41594-023-01128-y.

67. Ecker, K., Lorenz, A., Wolf, F., Ploner, C., Böck, G., Duncan, T., Geley, S., and Helmberg, A. (2009). A RAS recruitment screen identifies ZKSCAN4 as a glucocorticoid receptor-interacting protein. J. Mol. Endocrinol. *42*, 105–117. https://doi.org/10.1677/JME-08-0087.

68. Edwards, G.B., Muthurajan, U.M., Bowerman, S., and Luger, K. (2020). Analytical Ultracentrifugation (AUC): An Overview of the Application of Fluorescence and Absorbance AUC to the Study of Biological Macromolecules. Curr. Protoc. Mol. Biol. *133*, e131. https://doi.org/10.1002/cpmb.131.

69. Kingsbury, J.S., and Laue, T.M. (2011). Fluorescence-detected sedimentation in dilute and highly concentrated solutions. Methods Enzymol. *492*, 283–304. https://doi.org/10.1016/B978-0-12-381268-1.00021-5.

70. Kroe, R.R., and Laue, T.M. (2009). NUTS and BOLTS: applications of fluorescence-detected sedimentation. Anal. Biochem. *390*, 1–13. https://doi.org/10.1016/j.ab.2008.11.033.

71. Dahiya, V., Rutz, D.A., Moessmer, P., Mühlhofer, M., Lawatscheck, J., Rief, M., and Buchner, J. (2022). The switch from client holding to folding in the Hsp70/Hsp90 chaperone machineries is regulated by a direct interplay between co-chaperones. Mol. Cell *82*, 1543–1556.e6. https://doi.org/10.1016/j.molcel.2022.01.016.

72. Moessmer, P., Suren, T., Majdic, U., Dahiya, V., Rutz, D., Buchner, J., and Rief, M. (2022). Active unfolding of the glucocorticoid receptor by the Hsp70/Hsp40 chaperone system in single-molecule mechanical experiments. Proc. Natl. Acad. Sci. USA. *119*, e2119076119. https://doi.org/10.1073/pnas.2119076119.

73. Li, J., Richter, K., Reinstein, J., and Buchner, J. (2013). Integration of the accelerator Aha1 in the Hsp90 co-chaperone cycle. Nat. Struct. Mol. Biol. *20*, 326–331. https://doi.org/10.1038/nsmb.2502.

74. Alderson, T.R., Pritišanac, I., Kolarić, Đ., Moses, A.M., and Forman-Kay, J.D. (2023). Systematic identification of conditionally folded intrinsically disordered regions by AlphaFold2. Proc. Natl. Acad. Sci. USA. *120*, e2304302120. https://doi.org/10.1073/pnas.2304302120.

75. Perez-Riba, A., and Itzhaki, L.S. (2019). The tetratricopeptide-repeat motif is a versatile platform that enables diverse modes of molecular recognition. Curr. Opin. Struct. Biol. *54*, 43–49. https://doi.org/10.1016/j.sbi.2018.12.004.

76. Eckl, J.M., Drazic, A., Rutz, D.A., and Richter, K. (2014). Nematode Sgt1-homologue D1054.3 binds open and closed conformations of Hsp90 via distinct binding sites. Biochemistry *53*, 2505–2514. https://doi.org/10.1021/bi5000542.

77. Johnson, J.L., Zuehlke, A.D., Tenge, V.R., and Langworthy, J.C. (2014). Mutation of essential Hsp90 co-chaperones SGT1 or CNS1 renders yeast hypersensitive to overexpression of other co-chaperones. Curr. Genet. *60*, 265–276. https://doi.org/10.1007/s00294-014-0432-3.

78. Schuck, P. (2000). Size-distribution analysis of macromolecules by sedimentation velocity ultracentrifugation and lamm equation modeling. Biophys. J. *78*, 1606–1619. https://doi.org/10.1016/S0006-3495(00)76713-0.

79. Waterhouse, A.M., Procter, J.B., Martin, D.M.A., Clamp, M., and Barton, G.J. (2009). Jalview version 2—a multiple sequence alignment editor and analysis workbench. Bioinformatics *25*, 1189–1191. https://doi.org/10.1093/bioinformatics/btp033.

80. Shen, Y., and Bax, A. (2015). Protein structural information derived from NMR chemical shift with the neural network program TALOS-N. Methods Mol. Biol. *1260*, 17–32. https://doi.org/10.1007/978-1-4939-2239-0_2.

81. Delaglio, F., Grzesiek, S., Vuister, G.W., Zhu, G., Pfeifer, J., and Bax, A. (1995). NMRPipe: a multidimensional spectral processing system based on UNIX pipes. J. Biomol. NMR *6*, 277–293. https://doi.org/10.1007/BF00197809.

82. Vranken, W.F., Boucher, W., Stevens, T.J., Fogh, R.H., Pajon, A., Llinas, M., Ulrich, E.L., Markley, J.L., Ionides, J., and Laue, E.D. (2005). The CCPN data model for NMR spectroscopy: development of a software pipeline. Proteins *59*, 687–696. https://doi.org/10.1002/prot.20449.

83. Winn, M.D., Ballard, C.C., Cowtan, K.D., Dodson, E.J., Emsley, P., Evans, P.R., Keegan, R.M., Krissinel, E.B., Leslie, A.G.W., McCoy, A., et al. (2011). Overview of the CCP4 suite and current developments. Acta Crystallogr., D *67*, 235–242. https://doi.org/10.1107/S0907444910045749.

84. Nicholls, R.A., Long, F., and Murshudov, G.N. (2012). Low-resolution refinement tools in REFMAC5. Acta Crystallogr., D *68*, 404–417. https://doi.org/10.1107/S090744491105606X.

85. Emsley, P., Lohkamp, B., Scott, W.G., and Cowtan, K. (2010). Features and development of Coot. Acta Crystallogr., D *66*, 486–501. https://doi.org/10.1107/S0907444910007493.

86. McCoy, A.J., Grosse-Kunstleve, R.W., Adams, P.D., Winn, M.D., Storoni, L.C., and Read, R.J. (2007). Phaser crystallographic software. J. Appl. Crystallogr. *40*, 658–674. https://doi.org/10.1107/S0021889807021206.

87. Janke, C., Magiera, M.M., Rathfelder, N., Taxis, C., Reber, S., Maekawa, H., Moreno-Borchart, A., Doenges, G., Schwob, E., Schiebel, E., et al. (2004). A versatile toolbox for PCR-based tagging of yeast genes: new fluorescent proteins, more markers and promoter substitution cassettes. Yeast *21*, 947–962. https://doi.org/10.1002/yea.1142.

88. Gietz, R.D., and Schiestl, R.H. (2007). High-efficiency yeast transformation using the LiAc/SS carrier DNA/PEG method. Nat. Protoc. *2*, 31–34. https://doi.org/10.1038/nprot.2007.13.

89. Boeke, J.D., Trueheart, J., Natsoulis, G., and Fink, G.R. (1987). 5-Fluoroorotic acid as a selective agent in yeast molecular genetics. Methods Enzymol. *154*, 164–175. https://doi.org/10.1016/0076-6879(87)54076-9.

90. Ali, J.A., Jackson, A.P., Howells, A.J., and Maxwell, A. (1993). The 43-kilodalton N-terminal fragment of the DNA gyrase B protein hydrolyzes ATP and binds coumarin drugs. Biochemistry *32*, 2717–2724. https://doi.org/10.1021/bi00061a033.

91. Rutz, D.A., Luo, Q., Freiburger, L., Madl, T., Kaila, V.R.I., Sattler, M., and Buchner, J. (2018). A switch point in the molecular chaperone Hsp90 responding to client interaction. Nat. Commun. *9*, 1472. https://doi.org/10.1038/s41467-018-03946-x.

92. Sattler, M. (1999). Heteronuclear multidimensional NMR experiments for the structure determination of proteins in solution employing pulsed field gradients. Prog. Nucl. Magn. Reson. Spectrosc. *34*, 93–158. https://doi.org/10.1016/S0079-6565(98)00025-9.

93. Wishart, D.S., and Sykes, B.D. (1994). The 13C chemical-shift index: a simple method for the identification of protein secondary structure using 13C chemical-shift data. J. Biomol. NMR *4*, 171–180. https://doi.org/10.1007/bf00175245.

94. Lopez, A., Dahiya, V., Delhommel, F., Freiburger, L., Stehle, R., Asami, S., Rutz, D., Blair, L., Buchner, J., and Sattler, M. (2021). Client binding shifts the populations of dynamic Hsp90 conformations through an allosteric network. Sci. Adv. *7*, eabl7295. https://doi.org/10.1126/sciadv.abl7295.

95. Barbato, G., Ikura, M., Kay, L.E., Pastor, R.W., and Bax, A. (1992). Backbone dynamics of calmodulin studied by 15N relaxation using inverse detected two-dimensional NMR spectroscopy: the central helix is flexible. Biochemistry *31*, 5269–5278. https://doi.org/10.1021/bi00138a005.

96. Battiste, J.L., and Wagner, G. (2000). Utilization of site-directed spin labeling and high-resolution heteronuclear nuclear magnetic resonance for global fold determination of large proteins with limited nuclear overhauser effect data. Biochemistry *39*, 5355–5365. https://doi.org/10.1021/bi000060h.

97. Göbl, C., Madl, T., Simon, B., and Sattler, M. (2014). NMR approaches for structural analysis of multidomain proteins and complexes in solution. Prog. Nucl. Magn. Reson. Spectrosc. *80*, 26–63. https://doi.org/10.1016/j.pnmrs.2014.05.003.

98. Tessmer, M.H., and Stoll, S. (2023). chiLife: An open-source Python package for in silico spin labeling and integrative protein modeling. PLoS Comput. Biol. *19*, e1010834. https://doi.org/10.1371/journal.pcbi.1010834.

99. Williamson, M.P. (2013). Using chemical shift perturbation to characterise ligand binding. Prog. Nucl. Magn. Reson. Spectrosc. *73*, 1–16. https://doi.org/10.1016/j.pnmrs.2013.02.001.

100. Kabsch, W. (2010). XDS. Acta Crystallogr., D *66*, 125–132. https://doi.org/10.1107/s0907444909047337.

101. Evans, P.R., and Murshudov, G.N. (2013). How good are my data and what is the resolution? Acta Crystallogr., D *69*, 1204–1214. https://doi.org/10.1107/s0907444913000061.

STAR★METHODS

KEY RESOURCES TABLE

REAGENT or RESOURCE	SOURCE	IDENTIFIER
Antibodies		
Anti-GR	Sigma-Aldrich	Cat#: SAB4501309; RRID: AB_10744954
Anti-GAPDH	Origene	Cat#: AP21309AF-N; RRID:AB_10758142
Anti-SGT1	Pineda Research, Berlin	N/A
Anti-His6-Peroxidase	Roche	Cat#: 11965085001; RRID:AB_514487
Anti-HSP82	Pineda Research, Berlin	N/A
Anti-GR-LBD	Pineda Research, Berlin	N/A
IRDye_ 680RD Goat anti-Rabbit IgG Secondary Antibody	Licor	Cat#: 926-68071; RRID:AB_10956166
Bacterial and virus strains		
Rosetta (DE3)	Merck	Cat#: 70954-3
DH5alpha	New England Biolabs	Cat#: C2987H
Chemicals, peptides, and recombinant proteins		
Dexamethasone Fluorescein	Thermo Fisher Scientific	Cat#: D1383
Dexamethasone	Sigma-Aldrich	Cat#: D4902
ATP	Sigma-Aldrich	Cat#: A26209
ATPγS	Sigma-Aldrich	Cat#: A1388
Alexa Fluor 488 Malemid	Atto-Tec	Cat#: AD 488–45
Radicicol	Carl Roth	Cat#: HN72.3
5′fluorooroic Acid	Thermo Fisher Scientific	Cat#: R0812
Protease Inhibitor HP	SERVA electrophoresis	Cat#: 39106
3-(2-Iodacetamido)-PROXYL	Merck	Cat#: R426822
Pf1-Phages	ASLA biotech	Cat#: P-50-RNA
Lactate dehydrogenase	Sigma-Aldrich	Cat#: 10107085001
Pyrovate kinase	Sigma-Aldrich	Cat#: 10128155001
Protein G Sepharose™ 4 Fast Flow	GE Healthcare	Cat#: 17-0618-01
Deposited data		
Structure of Hsp82-MD/Sgt1-CS	This work	PDB: 9Q8O
Backbone resonance assignment of Sgt1-CSSGS	This work	BMRB: 53380
Experimental models: Organisms/strains		
Sgt1Δ BY4741; MATa; ura3Δ0; leu2Δ0; his3Δ1; met15Δ0; sgt1::hygNT [p416-GPD-SGT1]	This work	N/A
Sgt1-3 BY4741; MATa; ura3Δ0; leu2Δ0; his3Δ1; met15Δ0; sgt1-3::kanMX	Euroscarf	TSA830
WT Yeast BY4741; MATa; ura3Δ0; leu2Δ0; his3Δ1; met15Δ0	Euroscarf	Y00000
Oligonucleotides		
TTAAGGTTAAAGAGGTAGTTGTTTTAAGGA AACGAAAAAGAAATGcgtacgctgcaggtcgac	This work	S1_fw (N-terminal tagging of Sgt1)
ACTATATATCTACATATTGTAATTGTGTAGGTA TATACTAATCATTTAatcgatgaattcgagctcg	This work	S2_rev (C-terminal tagging of Sgt1)
Recombinant DNA		
p415-GPD-Sgt1 (UniProt ID: Q08446)	This work	N/A
p415-GPD-Sgt1-SGS	This work	N/A

(*Continued on next page*)

Continued

REAGENT or RESOURCE	SOURCE	IDENTIFIER
p415-GPD-Sgt1-CS	This work	N/A
p415-GPD-Sgt1-TPR	This work	N/A
p415-GPD-Sgt1-TPR-L-SGS	This work	N/A
p415-GPD-Sgt1-TPR-CS	This work	N/A
p415-GPD-Sgt1-CS-SGS	This work	N/A
p415-GPD- Sgt1-349-352Ala	This work	N/A
p415-GPD-Sgt1-M358P	This work	N/A
p415-GPD-Sgt1-F343P	This work	N/A
p415-GPD- Sgt1 1–371	This work	N/A
p415-GPD- Sgt1 1–372	This work	N/A
p415-NativePromoter-Sgt1	This work	N/A
p415-NativePromoter-Sgt1-CSSGS	This work	N/A
p415-NativePromoter-Sgt1-SGS	This work	N/A
p415-GPD-hSugt1A (UniProt ID: Q9Y2Z0-2)	This work	N/A
p415-GPD-hSugt1B (UniProt ID: Q9Y2Z0-1)	This work	N/A
p415-GPD-hSugt1-SGS	This work	N/A
p415-GPD-hSugt1-CS	This work	N/A
p415-GPD-hSugt1-TPR-B	This work	N/A
p416-Gal1-vSrc	Biebl et al. (2020)[32]	N/A
p413-GPD-GR (UniProt ID: P04150)	Schmid A, TU Munich	N/A
pET-Tev-Sgt1	This work	N/A
pETSumo-Sgt1-S233C	This work	N/A
pETSumo-Sgt1-SGS	This work	N/A
pETSumo-Sgt1-CS	This work	N/A
pETSumo-Sgt1-TPR	This work	N/A
pETSumo-Sgt1-CS-SGS	This work	N/A
pETSumo-Sgt1-TPR-CS	This work	N/A
pETSumo-Sgt1-1-371	This work	N/A
pETSumo-Sgt1-1-372	This work	N/A
pETSumo-Sgt1-CS-371	This work	N/A
pET-Sumo-Sgt1-CS-372	This work	N/A
pETSumo-Sgt1-SGS-M358P	This work	N/A
pETSumo-Sgt1-SGS-F343P	This work	N/A
pET28b-Sgt1	This work	N/A
pET28b-Hsp82 (UniProt ID: P02829)	Richter K, TU Munich	N/A
pETM11-Hsp82-NTD	Freiburger L, TU Munich	N/A
pETM11-Hsp82-MD	Freiburger L, TU Munich	N/A
pETM11-Hsp82-CTD	Freiburger L, TU Munich	N/A
pETSumo-hHsp70 (HSPA1A, UniProt ID: P0DMV8)	Kriehuber E., TU Munich	N/A
pETSumo-Ydj1 (UniProt ID: P25491)	Schmid A., TU Munich	N/A
pETHalo-GR-LBDm	Rutz D., TU Munich	N/A
pETSumo-Sti1 (UniProt ID: P15705)	Riedl M., TU Munich	N/A
pET28b-Sba1 (UniProt ID: P28707)	Richter K., TU Munich	N/A
pET28b-yAha1 (UniProt ID: Q12449)	Retzlaff M., TU Munich	N/A
Software and algorithms		
OriginPro	Originlab	https://www.originlab.com/
SedFit	Schuck (2000)[78]	http://www.rasmb.org/
Clustal Omega	EMBL-EBI	https://www.ebi.ac.uk/jdispatcher/msa/clustalo
Jalview	Waterhouse et al. (2009)[79]	https://www.jalview.org/

(*Continued on next page*)

Continued

REAGENT or RESOURCE	SOURCE	IDENTIFIER
PyMOL	Schrödinger	https://www.pymol.org/
BioRender	N/A	https://www.biorender.com/
TALOS-N	Shen and Bax (2015)[80]	https://spin.niddk.nih.gov/bax/software/TALOS-N/
NMRpipe	Delaglio et al. (1995)[81]	https://www.ibbr.umd.edu/nmrpipe/index.html
ccpNmr Analysis 2.5.2	Vranken et al. (2005)[82]	https://ccpn.info/software/version-2/version-2-downloads/
CCP4	Winn et al. (2011)[83]	https://www.ccp4.ac.uk/download/
REFMAC	Nicholls et al. (2012)[84]	N/A
Coot	Emsley et al. (2010)[85]	N/A
Phaser	McCoy et al. (2007)[86]	N/A

EXPERIMENTAL MODEL AND STUDY PARTICIPANT DETAILS

Yeast strains

All yeast strains used in this study are derivatives of BY4741 (MATa; ura3Δ0; leu2Δ0; his3Δ1; met15Δ0), and with the exception of the *sgt1Δ* strain, all strains were obtained from Euroscarf. Chromosomal deletion of Sgt1 was performed using a PCR-based method as described by Janke et al. (2004).[87] Specifically, the primers S1 and S2 were designed to replace the Sgt1 gene with the hphNT1 marker from the pFA6a-hphNT1 plasmid. The PCR product was used for yeast transformation, and colonies positive for the hphNT1 marker were confirmed by colony PCR.

METHOD DETAILS

Yeast transformation

Yeast strain transformation was performed as described by Gietz and Schiestl (2007),[88] in a slightly modified way. In brief, yeast cells were grown overnight in YPD medium and re-inoculated in 25 mL to a starting OD_{600} = 0.15. Yeast growth continued for approximately two cell division cycles at 30 °C (temperature-sensitive mutants were grown at 25 °C). Afterwards, cells were harvested (3000 x g for 5 min), washed once with water, once with 1 mL 0.1 M lithium acetate, and then resuspended in 0.5 mL 0.1 M lithium acetate. For each transformation, 50 µl cells were mixed with 240 µl PEG-3350 (50% w/v), 36 µl 1 M lithium acetate, 10 µl salmon sperm DNA (10mg/ml), and ~400 ng plasmid DNA adjusted with water to a total volume of 360µl. Samples were incubated at 30 °C for 30 min, heat-shocked at 42 °C for 30 min, pelleted (4000 × g, 30 s), and plated on selective medium.

Yeast viability assay

Yeast strains were grown overnight in selective media at 30 °C. 1 OD_{600} unit of cells was harvested, washed once with water, and resuspended in selective medium to an OD_{600} of 1. If not otherwise indicated, serial five-fold dilutions were prepared, and 5 µl of each dilution was spotted onto selective agar plates. Plates were incubated at 30 °C for 2 days before imaging.

Plasmid shuffling

The well-described method of 5-Fluoroorotic acid (5-FOA) plasmid shuffling was used to characterize the essential protein Sgt1.[89] The *sgt1Δ* p416-GPD-SGT1 strain was used for plasmid shuffling, in which the genomic copy of *SGT1* was deleted and replaced by a URA3-marked plasmid carrying a wild-type *SGT1* gene (p416-GPD-SGT1). The URA3 gene encodes orotidine-5'-phosphate decarboxylase which converts 5-FOA to the cell toxic 5-fluorouracil allowing counter-selection. The strain was transformed with a second plasmid containing Sgt1 mutants and plated on selective medium without 5-FOA. The plates were incubated for 3 days at 30 °C, and the appearing colonies were streaked out on plates containing 0.1% w/v 5-FOA to select for loss of the p416-GPD-SGT1 plasmid. The 5-FOA plates were incubated for 2–3 days at 30 °C prior to evaluation.

v-Src activity assay

Yeast strains carrying the *v-Src* gene under the control of the inducible GAL1 promoter were grown overnight at 25 °C in selective medium. 2 OD_{600} units of cells were harvested, washed once with water, and resuspended in selective medium. A total of 5 µl of yeast suspension at OD_{600} = 2 (for galactose plates) or OD_{600} = 0.04 (for glucose plates) was spotted onto selective agar plates containing either galactose or glucose. Plates were incubated at 25 °C for 2 days (glucose) or 4 days (galactose) before imaging.

GR stability analysis

BY4741 and *sgt1-3* yeast strains were grown overnight at 25 °C in selective medium. Cells were re-inoculated at OD_{600} = 0.15 in 10 ml selective medium and cultured for 8 h at 25 °C. Cultures were then shifted to 30 °C and incubated overnight. Cells were re-inoculated at OD_{600} = 0.3 and grown for 6 h at 30 °C. A total of 5 OD units of cells were harvested and lysed using the alkali lysis method. The resulting pellet fraction was solubilized in Laemmli buffer and analyzed using western blotting.

Co-immunoprecipitation

The wild-type yeast strain BY4741 was grown overnight in YPD medium at 30 °C. Cells were re-inoculated at OD_{600} = 0.15 and grown to the exponential phase (OD_{600} = 0.8–1.2). A total of 50 OD units were harvested, washed twice with PBS, and resuspended in lysis buffer (50 mM Tris, pH 8.0, 300 mM NaCl, 1% NP-40 substitute, Protease Inhibitor Mix FY). From this step onward, all procedures were carried out at 4 °C. Cells were disrupted with glass beads using a shaker mill (4 × 3 min, 50% frequency), and lysates were cleared by centrifugation (10 min, 14,000 rpm). Protein concentration was adjusted to 1 mg/ml.

Lysates were pre-cleared with 10 μl Protein G–Sepharose (50% slurry) beads per 0.5 ml lysate for 1 h. After bead removal, 10 μg His-Sgt1 and 3 μg GR-LBD were added and incubated for 1 h. For immunoprecipitation, 3 μl anti-Sgt1 antibody was added for 1 h, followed by 30 μl Protein G–Sepharose beads for an additional 1 h. A beads-only sample served as a negative control. Beads were washed three times with lysis buffer and once with 50 mM Tris, pH 8.0. Bound proteins were eluted in 40 μl buffer (50 mM Tris, pH 7.5, 1% SDS, 100 mM DTT) by heating at 95 °C for 3 min. Eluates were mixed with 5× Laemmli buffer and analyzed by western blotting.

Protein expression, purification, and labeling

Yeast Sgt1, Sgt1 mutants and domains, Hsp82 domains, Sti1, Ydj1, and human Hsp70 were expressed with a 6xHis-SUMO tag or a 6xHis-TEV tag in *E. coli* Rosetta cells. Harvested cells were lysed by sonication in NiNTA buffer A (50 mM Na_2HPO_4, pH 7.5, 300–500 mM NaCl, 10 mM imidazole, 1 mM DTT + Protease Inhibitor HP, 2 mM PMSF). Lysates were cleared at 40,000 g for 1 h. Cleared lysates were subjected to affinity chromatography on a HisTrap FF column (Cytiva). Bound protein was washed with 2 mM ATP dissolved in NiNTA buffer A before elution with NiNTA buffer B containing 300 mM imidazole. The elute fractions were pooled, and the SUMO tag was cleaved by the addition of Ulp1 or Tev protease (depending on the construct) and dialyzed in NiNTA A buffer overnight at 4 °C. To get rid of the SUMO-/His-tag and the protease, the digested protein was run again over a His-Trap FF column, and the flow-through was collected. Hsp82 and full-length Sgt1 were diluted with Resource Q buffer A (40 mM HEPES, pH 7.5, 20 mM KCl, 1 mM EDTA, 1 mM DTT) to a salt concentration lower than 50 mM and loaded onto a Resource Q ion-exchange column. Elution of the bound proteins was done using a continuous salt gradient of Resource Q buffer B (40 mM HEPES, pH 7.5, 1 M KCl, 1 mM EDTA, 1 mM DTT). Subsequently, all proteins were subjected to size exclusion chromatography in SEC buffer (40 mM HEPES, pH 7.5, 150 mM KCl, 5 mM $MgCl_2$, 1 mM DTT). Yeast Hsp82, Sba1, Aha1 and Sgt1 used for co-immunoprecipitation were expressed with a C-terminal 6xHis-tag. Affinity chromatography was performed as described above. Subsequently, the proteins were directly subject to ion-exchange and size exclusion chromatography. All experiments with GR-LBD were conducted with the stabilized GR-LBDm construct (aa 527–777, F602S/A605V/V702A/E705G/M752T). The protein was expressed in *E. coli* Rosetta cells in self-induction medium (16 h, 16 °C). Harvested cells were resuspended in lysis buffer (50 mM Tris pH 7.9, 2 M urea, 100 mM NaCl, 5 mM $MgCl_2$, 10 mM imidazole, 2 mM β-mercaptoethanol, 50 μM DEX) supplemented with DNase I and Protease Inhibitor HP, lysed by sonication, and cleared by centrifugation (40,000 g, 1 h). The lysate was loaded onto a HisTrap FF column (Cytiva), washed with a 0-100% gradient of NiNTA-A buffer (50 mM Tris pH 7.9, 500 mM NaCl, 10 mM imidazole, 10% glycerol, 2 mM β-mercaptoethanol, 50 μM DEX), and eluted with NiNTA-B buffer (350 mM imidazole). Pooled fractions were digested with TEV protease during overnight dialysis (50 mM Tris pH 7.9, 100 mM NaCl, 10% glycerol, 2 mM β-mercaptoethanol, 0.5% CHAPS, 50 μM DEX) at 4 °C and passed over a HisTrap FF column to remove the protein tag and TEV. The flow-through was concentrated and purified by size exclusion chromatography in GR storage buffer (25 mM Tris pH 7.9, 100 mM NaCl, 10% glycerol, 2 mM DTT, 50 μM DEX). Peak fractions containing pure protein were pooled and concentrated. Apo GR-LBD was generated by two rounds of dialysis of holo GR-LBD against ligand-free buffer (50 mM Tris pH 7.9, 100 mM NaCl, 10% glycerol, 2 mM β-mercaptoethanol, 0.5% CHAPS).

Proteins were fluorescently labeled with maleimide-Atto488. For Sgt1, the cysteine mutant *S233C* was used, as the native cysteines are poorly accessible for labeling. Other proteins were labeled without additional cysteine mutations. Proteins were dialyzed into a non-reducing reaction buffer (40 mM HEPES, pH 7.5, 150 mM KCl, 5 mM $MgCl_2$). The dye was added to a molar ratio of protein:dye (1:2) and incubated for 1–2 h at RT. The reaction was quenched by adding 5 mM DTT. Free dye was separated by a Sephadex® column (10 mm x 300 mm) using SEC buffer (40 mM HEPES, pH 7.5, 150 mM KCl, 5 mM $MgCl_2$, 1 mM DTT).

Analytical ultracentrifugation

Sedimentation velocity experiments were performed using a ProteomLab Beckman XL-A centrifuge (Beckman Coulter, Brea, California) equipped with an AVIV fluorescence detection system (Aviv biomedical Inc., Lakewood, USA). Experiments were performed at 42,000 rpm and 20 °C in an eight-hole Ti-50 Beckman Coulter rotor. 300 scans were recorded, in a total measurement time of 6h. 500 nM Atto488 labeled protein was detected in AUC buffer (20 mM HEPES, pH 7.5, 20 mM KCL, 5 mM $MgCl_2$). All other protein concentrations were used as indicated in the figure legends. Nucleotides were added to a concentration of 5 mM (ATP) and 2 mM (ATPγS). Sedfit and OriginPro 2024 were used for data analysis. The data was normalized to the total area under the curve, whereby peaks of free label were excluded from the calculation. Normalized c(S) distributions were plotted against the sedimentation

coefficient S. To quantify the percentage of specific complexes, normalized data were used, and the area under the peak of the desired complex was determined.

To determine the dissociation constant (K_D) of Sgt1 and Hsp82, the percentage of bound species was quantified by calculating the area under the Hsp82/Sgt1 complex. The concentration of Hsp82 was plotted against the percentage of bound species. The Hill1 fit was used to determine the K_D and the Hill coefficient (N). Mean±Standard deviation was determined by three individual experiments.

Fluorescence polarization measurement

Hormone binding to the GR-LBD was carried out essentially as described previously.[60] Briefly, for equilibrium GR-LBD measurements, 1 μM of apo GR-LBD was mixed with different combinations of the following protein: 2 μM Hsp40 (Ydj1), 10 μM hHsp70, 4 μM Hsp90 (Hsp82), 12 μM Sgt1 and 5 mM ATP in 40 mM HEPES pH 7.5, 150 mM KCl, 5 mM $MgCl_2$, 2 mM DTT buffer. The proteins were incubated at room temperature for 60 min. F-Dex was added in a final concentration of 100 nM, and the binding of F-Dex to the GR-LBD was monitored at 30 °C by measuring the fluorescence polarization values. For the analysis, the start value immediately after the addition of F-Dex was subtracted from the trace. The mean of the last 10 values was used to calculate the endpoints of each measurement.

ATPase assay

The Hsp82 ATPase activity was measured with a regenerative ATPase assay as previously published.[90,91] Briefly, assay buffer was prepared containing 5.17 mM phosphoenolpyruvate (PEP), 0.43 mM nicotinamide adenine dinucleotide (NADH), 5.17 U/mL pyruvate kinase (PK) and 26.06 U/mL lactate dehydrogenase (LDH) in 40 mM HEPES, pH 7.5, 150 mM KCl, 5 mM $MgCl_2$. Assay buffer was mixed 1:1 with proteins diluted in 40 mM HEPES, pH 7.5, 150 mM KCl, 5 mM $MgCl_2$, and incubated for 30 min at 30 °C. Concentrations of the proteins were used as indicated. The reaction was initiated by the addition of 5 mM ATP, and the absorption at 340 nm was continuously recorded at 30 °C. To assess potential contaminating ATPase activities that might co-purify with the proteins, each protein batch was tested for intrinsic ATPase activity under identical experimental conditions. Hsp90 was tested under the addition of radicicol, a specific inhibitor of Hsp90 ATPase. A minor background rate was only detected for Sgt1-TPR-CS. The background activity was subtracted from the corresponding Hsp90 measurements. ATPase turnover rates (per Hsp90 dimer per minute) were calculated according to the Beer–Lambert law.

Western blot

Samples were subjected to SDS–PAGE (SERVAGel™ TG PRiME™ 4%–20%) and transferred onto a PVDF membrane. Primary antibodies were used at the following dilutions: Anti-GR (1:500); Anti-SGT1, Anti-GAPDH, Anti-GR-LBD, and Anti-His6-Peroxidase (1:1000); Anti-HSP82 (1:5000). If required, peroxidase-coupled secondary antibodies were applied. Protein bands were visualized using the ImageQuant LAS 4000 imaging system. Quantification of immunoblots was performed using GelAnalyzer 23.1.

Circular dichroism spectroscopy

Far-UV CD spectra were recorded from 200 to 260 nm on a Chirascan-plus spectrometer (Applied Photophysics, Leatherhead, England). Measurements were performed at 30 °C using a bandwidth of 1 nm, a step size of 1 nm, and an integration time of 0.5 s per point. Protein samples (0.1 mg/ml) were measured in a quartz cuvette with a 1 mm path length. For each sample, 10 individual scans were averaged.

NMR

All NMR experiments were performed on Bruker Avance spectrometers equipped with cryogenically cooled TCI probe heads, operating at magnetic field strengths corresponding to ^1H Larmor frequencies of 600 to 1200 MHz. The sample temperature was set at 298 K for all experiments unless otherwise specified. ^1H,^{15}N correlation experiments were performed in 40 mM phosphate buffer, 100 mM NaCl, 2 mM DTT, pH 6.8, 8% D_2O, while methyl-labeled experiments were all performed in 20 mM tris-D_{11}, 100 mM NaCl, 5 mM $MgCl_2$, 2 mM DTT-D_{10}, 0.02% NaN_3, pH 7, in 99.9% D_2O. All data were processed with NMRpipe[81] and analyzed in CCPNMR.[82]

Chemical shift assignments

The backbone assignment of all Sgt1 constructs was performed using standard 3D heteronuclear experiments HNCACB, HNCA, CBCA(CO)NH or (H)C(CCO)NH, HNCO and HN(CA)CO.[92] The combined ^{13}Ca, ^{13}Cb, $^{13}C'$ secondary shifts ($\Delta\delta_{av}(^{13}C)$) were calculated as $[\Delta\delta(^{13}C\alpha) - \Delta\delta(^{13}C\beta) + \Delta\delta(^{13}C')]$, where $\Delta\delta$ is the difference between observed ^{13}C chemical shifts and random coil values. Since $\Delta\delta(^{13}C\alpha)$ and $\Delta\delta(^{13}C')$ are positive and $\Delta\delta(^{13}C\beta)$ is negative in helical conformations and opposite in strand conformations, the value $\Delta\delta_{av}(^{13}C)$ can be used to evaluate secondary structure propensity.[93] Methyl-labeled samples were prepared as previously described. Backbone and methyl resonances of Hsp82 were previously assigned by us.[33,94] The $\{^1H\}$-^{15}N heteronuclear NOE were recorded as described[95] in an interleaved manner with a recycling time of 4s.

Paramagnetic relaxation enhancements (PRE)

The mutant Sgt1-SGS E375C was first exchanged to an NMR-buffer without DTT using a PD10 buffer exchange column (GE Healthcare, Buckinghamshire, UK). Two other mutants were generated (344C and 366C) but were not included as they significantly affected the ^{1}H-^{15}N HSQC spectra of SGT1-SGS and thus likely affected its conformational state. IPSL (N-(1-oxyl-2,2,5,5-tetramethyl-3-pyrrolidinyl)iodoacetamide) was added to a 10 times molar excess to Sgt1-SGS E375C in non-reduced buffer and incubated overnight at room temperature and protected from light. The excess spin label was removed using a PD10 column. 200 μM of Sgt1-SGS E375C IPSL-labeled was prepared and measured. Data were recorded using ^{1}H,^{15}N HSQC experiment with a recycling delay of 4s. 10 times molar excess of fresh ascorbic acid was added to reduce the paramagnetic probe, and the experiment was repeated using the same parameters to record the reference experiment in the absence of PRE.[96,97] Theoretical PRE effects on Sgt1-SGS E375C were calculated based on the AF2 model from the AF-PSD (AF-Q08446-F1-v4). Seven different conformations of IPSL covalently bound to C375 were generated using the python package chiLife.[98] For each structure and conformation, the distance between the paramagnetic center and the backbone NH of Sgt1-SGS S375C were extracted in pymol using the distancetoatom script. The relaxation ratio was calculated as described[96] for each conformation, assuming a tumbling correlation τ_c of 50 ns, an ^{1}H-R_2 transverse relaxation rate of 80 s^{-1}, and a total INEPT evolution time of 9 ms.

Residual dipolar couplings

^{1}H-^{15}N residual dipolar couplings (RDCs) were obtained by recording IPAP-HSQC experiments on ^{15}N-labeled samples of Sgt1-SGS at 270 μM concentration, in absence and in presence of 12.5 mg/mL of Pf1-phages (ASLA biotech). The alignment was confirmed by ^{2}H 1D NMR that showed a deuterium splitting value of around 9 Hz.

Titrations

Titration of the ^{15}N-labeled Sgt1-CS-SGS were performed at 100 μM with either 2-points titration 1:0.5 and 1:1 for Hsp90-FL, Hsp90-CTD and GR or 7-point titrations for Hsp90-NTD and Hsp90-Md. Reported CSPs on the figure correspond to the 1:1 ratios. Perturbations and intensity changes on methyl-labeled Hsp90 were performed at 300 μM with a single addition of Sgt1 constructs at 450 μM. Titrations were performed with proteins purified in identical buffers. The assignment of fully bound-forms, used to determine chemical shifts perturbations, was performed from the successive addition of binding partners and following the chemical shift perturbations. All chemical shift perturbations were calculated as a weighted average following the equations $CSP = ((\Delta\delta^{1}H)^2 + (\Delta\delta^{15}N*0.15)^2)^{1/2}$ for ^{1}H, ^{15}N spectra and $CSP = ((\Delta\delta^{1}H)^2 + (\Delta\delta^{13}C*0.3)^2)^{1/2}$ for ^{1}H, ^{13}C spectra.[99]

Crystallography

Initial screening of crystallization conditions was carried out by the vapor diffusion method. Sitting drops were set up using 400 nL of a 1:1 mixture of protein and crystallization solutions. The co-crystallization was performed using Hsp90-MD and Sgt1-CS with a complex concentration of 20 mg/mL. Crystals were obtained at 20 °C from a solution containing 0.04 M Magnesium chloride, 0.05 M Sodium cacodylate, 5% v/v 2-Methyl-2,4-pentanediol. Single crystals were cryoprotected using 25% glycerol in the mother solution and flash-frozen in liquid nitrogen. The diffraction data were collected at the X06DA beamline at the Swiss Light Source (Paul Scherrer Institut, Villigen, Switzerland). The data were indexed and integrated using the XDS program package[100] and scaled and merged using the Aimless program[101] The initial phases were obtained by molecular replacement, calculated using Phaser software[86] using Hsp90-MD structure (pdb:1HK7[34]) and the Sgt1-CS from Arabidopsis thaliana (pdb:2JKI[45]). All crystallographic calculations were carried within the CCP4 program suite.[83] The protein structure was refined with the program REFMAC[84] and manual adjustments were made to the models using Coot.[85] Atomic coordinates and structure factors for the Hsp90-MD/Sgt1-CS complex have been deposited in the RCSB Protein Data Bank with pdb code 9Q8O.

QUANTIFICATION AND STATISTICAL ANALYSIS

Details of statistical tests and the exact number of replicates (n) are provided in the corresponding figure legends. All analyses were performed using OriginPro 10.2. Statistical significance was defined as follows: ns, $p \geq 0.05$; *$p < 0.05$; **$p < 0.01$; ***$p < 0.001$; ****$p < 0.0001$.